FERMILAB-PUB-12-048-T

Exploring ν signals in dark matter detectors

Roni Harnik[1],* Joachim Kopp[1],† and Pedro A. N. Machado[1,2,3‡]

[1] *Fermilab, P.O. Box 500, Batavia, IL 60510-0500, USA*
[2] *Instituto de Física, Universidade de São Paulo, C.P. 66.318, 05315-970 São Paulo, Brazil*
[3] *Institut de Physique Théorique, CEA Saclay, 91191 Gif-sur-Yvette, France*

(Dated: February 27, 2011)

We investigate standard and non-standard solar neutrino signals in direct dark matter detection experiments. It is well known that even without new physics, scattering of solar neutrinos on nuclei or electrons is an irreducible background for direct dark matter searches, once these experiments reach the ton scale. Here, we entertain the possibility that neutrino interactions are enhanced by new physics, such as new light force carriers (for instance a "dark photon") or neutrino magnetic moments. We consider models with only the three standard neutrino flavors, as well as scenarios with extra sterile neutrinos. We find that low-energy neutrino–electron and neutrino–nucleus scattering rates can be enhanced by several orders of magnitude, potentially enough to explain the event excesses observed in CoGeNT and CRESST. We also investigate temporal modulation in these neutrino signals, which can arise from geometric effects, oscillation physics, non-standard neutrino energy loss, and direction-dependent detection efficiencies. We emphasize that, in addition to providing potential explanations for existing signals, models featuring new physics in the neutrino sector can also be very relevant to future dark matter searches, where, on the one hand, they can be probed and constrained, but on the other hand, their signatures could also be confused with dark matter signals.

PACS numbers:

1. INTRODUCTION AND MOTIVATION

Experiments searching for dark matter and those studying solar neutrinos have coexisted for many years, and even though many of the technological challenges—such as the suppression of radioactive backgrounds and the lowering of the energy threshold—are similar for both types of experiments, their physics programs have had little overlap. In solar neutrino physics, the size of the detector is more important than the energy threshold, whereas the direct search for dark matter scattering is only possible for low energy thresholds of order 10 keV or below. Until very recently, achieving such a low threshold has only been possible in small detectors with masses of only a few kg, too small to be of interest to neutrino physics. However, as dark matter detectors are becoming more and more massive, this is about to change. In ton scale experiments, solar neutrinos will constitute a non-negligible irreducible background [1] which can only be overcome in detectors with directional sensitivity.

In this work we consider the additional possibility that there is new physics in the neutrino sector, and we will examine how this may affect the signals observed by present and future dark

*Email: roni@fnal.gov
†Email: jkopp@fnal.gov
‡Email: accioly@fma.if.usp.br

Operated by Fermi Research Alliance, LLC under Contract No. De-AC02-07CH11359 with the United States Department of Energy.

matter experiments. In particular, we will discuss models featuring a new light ($\ll 1$ GeV) gauge boson A'. We will also discuss the possible existence of neutrino magnetic moments and of extra ("sterile") neutrino species coupled to the new gauge boson.[1] Sterile neutrinos are motivated by a number of anomalous results from short-baseline neutrino oscillation experiments [2–11] and by cosmology [12–14], whereas new light force carriers appear for instance in models of Sommerfeld-enhanced dark matter annihilation (see e.g. [15–19]). Both sterile neutrinos and light force carriers were used by Nelson and Walsh to explain some of the neutrino oscillations anomalies [20, 21] (see also [22] for related work). As also pointed out by Pospelov [23], a new light force carrier can enhance the interaction rates of active and sterile neutrinos at low energy by several orders of magnitude compared to Standard Model neutrinos. Additionally, it can have a large impact on the Mikheyev-Smirnov-Wolfenstein (MSW) potential that neutrinos feel when propagating through matter, thus affecting oscillations.

As examples, we will consider potential explanations of current dark matter anomalies, in particular the event excesses observed by CoGeNT [24, 25] and CRESST [26], as well as the annual modulation signals observed in CoGeNT [25] and DAMA [27]. While we will see that finding a model that is consistent with all current direct detection data and with constraints from neutrino oscillation experiments is difficult (a fate that our scenario shares with most dark matter models), we will also see that future experiments can be considerably affected by new physics in the neutrino sector. In particular, neutrino signals beyond from physics beyond the Standard Model may be confused with genuine dark matter signals. (The problem of other types of new physics faking a dark matter signal is well-known in the context of collider searches [28–31] but has received less attention in the framework of direct searches.)

It will be important for us that dedicated neutrino experiments have a much higher energy threshold than dark matter detectors, which can detect electron recoil energies as low as 0.5 keVee and nuclear recoil energies down to 2 keVnr[2] in the case of CoGeNT [24] and CDMS [32]. Thus, if new physics in the neutrino sector manifests itself most strongly at low energy, neutrino detectors would be insensitive, while dark matter detectors have excellent prospects of discovering or constraining such models.

The outline of the paper is as follows: In section 2, we review neutrino scattering in the Standard Model and compute the expected neutrino–electron and neutrino–nucleus scattering rates in dark matter detectors. We then introduce in section 3 four representative extension of the Standard Model that can lead to enhanced neutrino interactions at low energy. In particular, we will discuss neutrino magnetic moments, light new gauge bosons with various coupling structures, and sterile neutrinos. The phenomenology of these models is then analyzed in section 4 with regard to neutrino–electron scattering and in section 5 with regard to neutrino–nucleus scattering. In section 6, we discuss several mechanisms that can lead to diurnal, semi-annual and annual modulation of the neutrino count rate at the Earth: The varying Earth–Sun distance, oscillation with very long (~ 1 AU) oscillation length, Earth matter effects, sterile neutrino absorption, and direction-dependent detection efficiencies. Finally, in section 7, we discuss existing experimental limits on light gauge bosons, and we show how they constrain the models introduced earlier. We also use Borexino and GEMMA data to set new limits on models with light force carriers. We summarize

[1] In a slight abuse of nomenclature, we will call the extra neutrino flavors "sterile" even though they can interact with ordinary matter through A' exchange.

[2] The notation keVee refers to the "electron equivalent energy in keV", which is defined as the reconstructed recoil energy under the assumption that it is carried by an electron. For nuclear recoils, only part of the recoil energy is visible in the detector—an effect which has to be corrected for by dividing the visible energy by a quenching factor—so that the energy threshold for nuclear recoils is higher than that for electron recoils. When referring to a nuclear recoil energy, we will use the notation "keVnr".

and conclude in section 8.

2. NEUTRINO INTERACTIONS IN DARK MATTER DETECTORS IN THE STANDARD MODEL

Solar neutrinos may scatter elastically with nuclei or with electrons in a target and produce low energy recoil events. Within the Standard Model [33], the interaction rates are very low, beyond the reach of current and near future dark matter detectors, but well within the reach of the larger dedicated solar neutrino experiments Borexino [34] and SNO [35, 36]. Solar neutrino interactions will also become relevant to dark matter experiments once these experiments reach a sensitivity to dark matter–nucleon scattering cross sections of order 10^{-46} cm^2 [1].

The differential cross section for neutrino–electron scattering in the Standard Model is easily found to be

$$\frac{d\sigma_{\rm SM}(\nu_e e \to \nu_e e)}{dE_r} = \frac{G_F^2 m_e}{2\pi E_\nu^2}\Big[4s_w^4(2E_\nu^2 + E_r^2 - E_r(2E_\nu + m_e)) - 2s_w^2(E_r m_e - 2E_\nu^2) + E_\nu^2\Big]\,, \quad (1)$$

$$\frac{d\sigma_{\rm SM}(\nu_{\mu,\tau} e \to \nu_{\mu,\tau} e)}{dE_r} = \frac{G_F^2 m_e}{2\pi E_\nu^2}\Big[4s_w^4(2E_\nu^2 + E_r^2 - E_r(2E_\nu + m_e)) + 2s_w^2(E_r m_e - 2E_\nu^2) + E_\nu^2\Big] \quad (2)$$

for electron neutrinos (ν_e) and muon/tau neutrinos (ν_μ, ν_τ), respectively. In these expressions, G_F is the Fermi constant, s_w is the sine of the Weinberg angle, E_ν and E_r are the neutrino energy and the recoil energy transferred to the target electron, respectively, and m_e is the electron mass. Note that scattering of electron neutrinos on electrons receives contributions from s-channel W exchange and from t-channel Z exchange, whereas for muon and tau neutrinos, only Z exchange is possible. The differential cross section for neutrino–nucleus scattering is

$$\begin{aligned}\frac{d\sigma_{\rm SM}(\nu_{e,\mu,\tau} N \to \nu_{e,\mu,\tau} N)}{dE_r} = \frac{G_F^2 m_N F^2(E_r)}{2\pi E_\nu^2}\Big[&A^2 E_\nu^2 + 2AZ(2E_\nu^2(s_w^2 - 1) - E_r m_N s_w^2) \\ &+ 4Z^2(E_\nu^2 + s_w^4(2E_\nu^2 + E_r^2 - E_r(2E_\nu + m_N)) + s_w^2(E_r m_N - 2E_\nu^2))\Big]\,,\end{aligned} \quad (3)$$

for a nucleus of mass m_N, nucleon number A and charge Z. The function $F(E_r)$ is the nuclear form factor, for which we will use the form $F(E_r) = 3e^{-\kappa^2 s^2/2}[\sin(\kappa r) - \kappa r\cos(\kappa r)]/(\kappa r)^3$, with $s = 1$ fm, $r = \sqrt{R^2 - 5s^2}$, $R = 1.2A^{1/3}$ fm, $\kappa = \sqrt{2m_N E_r}$ (and $q^2 \simeq -\kappa^2$) [37]. Note that for heavy nuclei low-energy neutrino–nucleus scattering is enhanced compared to scattering on light nuclei because the cross section contains terms proportional to A^2, Z^2 and AZ. These terms reflect the fact that neutrinos scatter coherently off all the nucleons. At higher recoil energies, the form factor becomes relevant and compensates part or all of this enhancement.

The maximum recoil energy of a target particle of mass m_T for fixed E_ν is given by

$$E_r^{\rm max} = \frac{2E_\nu^2}{m_T + 2E_\nu}\,, \quad (4)$$

and, conversely, the minimum neutrino energy required for transferring a given recoil energy E_r is

$$E_\nu^{\rm min} = \frac{1}{2}\left(E_r + \sqrt{E_r^2 + 2E_r m_T}\right)\,. \quad (5)$$

For $m_T \gg E_r$, the case we will mostly be concerned with in this paper, we can make the approximation $E_\nu^{\rm min} \simeq \sqrt{m_T E_r/2}$. The event rate at a detector is obtained by folding $d\sigma/dE_r$ with the

solar neutrino flux $d\Phi/dE_\nu$:

$$\frac{dR}{dE_r} = N_T \int_{E_\nu^{\min}}^{\infty} \frac{d\Phi}{dE_\nu} \frac{d\sigma}{dE_r}\, dE_\nu \,, \tag{6}$$

where N_T is the number of target particles in the experiment.

In order for a nucleus of mass m_N to receive a recoil energy $E_r \sim$ few keV (above the threshold of dark matter detectors), the neutrino must have an energy $E_\nu \gtrsim \sqrt{E_r m_N/2} \sim$ few MeV. Only the high energy tail of the solar neutrino spectrum exceeds this threshold, so the rate of nuclear recoil events is low. On the other hand, the requirement for an electron recoil above threshold is only $E_\nu \gtrsim$ few $\times$ 10 keV, allowing for most of the solar neutrino flux to contribute. As a result, the spectrum of solar neutrino-induced electron recoil events in a dark matter detector with a threshold of few to 10 keV is dominated by the low-energy *pp* neutrinos ($E_\nu < 420$ keV), whereas nuclear recoils are mostly induced by ^{8}B neutrinos ($E_\nu \lesssim 15$ MeV).

The Standard Model neutrino–electron and neutrino–nucleus scattering rates are plotted in figure 1 and compared to the event rates observed in several dark matter detectors and neutrino experiments. Note that the neutrino–nucleus scattering rate at any given recoil energy depends on the target material. In figure 1b, we have chosen germanium as an example, see [1] for plots of scattering rates on different nuclear targets. Note also that we neglect the fact that the electrons and nuclei in the target material are in bound states. This is justified because their binding energies are in most cases much smaller than the $\mathcal{O}$(keV) recoil energies we are interested in.[3] The only exception are the very inner electrons in the case of a heavy target material, which can have binding energies of order 10 keV. We have checked that including the effects of electron wave functions in our calculation leads only to a correction to the predicted neutrino–electron scattering rate of at most few–20% and introduces small spectral features at those energies where additional electron shells become kinematically accessible. By neglecting these small corrections, our results for neutrino–electron scattering become material-independent and can thus be directly applied to any dark matter direct detection experiment.

In this paper we will consider a variety of new physics scenarios which add a new contribution to the differential cross section in the integrand of equation (6). Obviously we will need to take care and respect all limits from existing measurements of the solar neutrino flux, as well as other neutrino experiments. It is thus useful to review the most important constraints:

Neutrino–electron interactions:
For neutrino–electron scattering (figure 1a), the strongest limits on any anomalous contribution to the cross section comes from Borexino [34] and SNO [35, 36], which have energy thresholds of $\sim$ 250 keV and 6 MeV, respectively. This leaves little room for new physics at $E_r \gtrsim 200$ keV. At lower energies the electron recoil event rates observed in the dark matter experiments XENON-100 [39], DAMA [40] and CoGeNT [25] lie 3 to 5 orders of magnitude above the Standard Model solar neutrino background, so that a substantial enhancement of the neutrino–electron scattering rate cannot be excluded there. The most constraining measurement is by XENON-100, but we should stress that the precise energy threshold and rate for electron recoils below $E_r \lesssim$ few $\times$ 10 keV in XENON-100 are not precisely known since electron recoils are not relevant to XENON-100's dark matter search except as a background. The energy calibration for electron recoils depend on the light yield L_y, which gives the number of detected scintillation photons as a function of

[3] This is different for the scattering of dark matter with a mass $\gtrsim$ 1 GeV on electrons, where observable recoil energies can occur only when the electron enters the scattering process with a large initial momentum of at least a few MeV. In this case, a dark matter detector would be probing the high-momentum tail of the bound state electron wave functions, and, consequently, the fact that electrons are bound cannot be neglected [38].

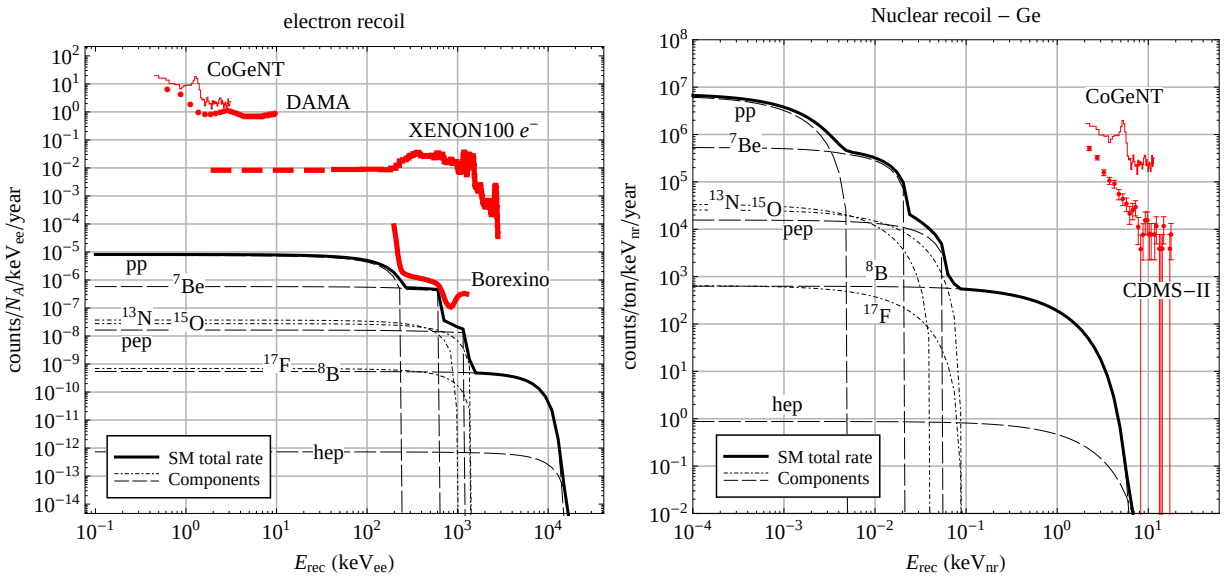

Figure 1: Expected event rates in dark matter detectors from (a) solar neutrino–electron scattering and (b) solar neutrino–nucleus scattering in germanium. In (a), we use units of events per keVee per year per N_A electrons (where N_A is the Avogadro number) to be able to compare rates in different materials. Thick black lines correspond to the total event rate, while thin lines break the rate up into contributions from different neutrino production processes. We also show the observed electron recoil spectra in XENON-100 [39] (see text for details) and Borexino [34], from the low-threshold analysis of CDMS data [32], and the event spectra from CoGeNT [25] and DAMA [40]. Since CoGeNT and DAMA cannot distinguish nuclear recoils from electron recoils, we interpret their data as electron recoil in the left panel and as nuclear recoils in the right panels.

the electron recoil energy, and which was only measured at higher energies (122 keV) and has to be extrapolated down to lower energies. In figure 1a we have used XENON-100's working assumption that the light yield at low energies is the same as in the calibration measurement at $E_r = 122$ keV, $L_y = 2.2$ PE/keVee, which leads to a detection threshold for electron recoils of about 2 keVee. Measurements indicate that the light yield might actually be larger at lower recoil energies (down to 30 keVee) [41], and if this trend continues to even lower recoil energies, the energy threshold in XENON-100 might be even lower (and the background rate per keVee somewhat higher) than what is shown in figure 1a. However, in many scintillators the light yield peaks at $E_r \sim 10$ keVee and drops steeply below [41], so that the exact sensitivity of the XENON-100 detector to low-energy electron recoil events remains somewhat uncertain. In figure 1, as well as figures 2 and 3, we indicate this uncertainty by a dashed red lines below $E_r = 50$ keVee. Besides Borexino and XENON-100, also the GEMMA experiment [42] has placed limits on neutrino–electron scattering at low recoil energies. GEMMA limits are not directly comparable to to the limits shown in figure 1 because GEMMA used not solar neutrinos, but reactor anti-neutrinos, and thus the neutrino spectrum was different. We will comment more on GEMMA in section 4 when discussing neutrino magnetic moments, and also in section 7.

Neutrino–nucleus interactions:
For neutrino–nucleus scattering (figure 1b), we compare the Standard Model prediction to the observed event rates in CoGeNT [25] and CDMS [32]. Here we discuss only *elastic* neutrino–nucleus scattering because it has been shown in [23] that the new physics contributions to the cross sections for inelastic processes like neutrino-induced deuteron breakup or nuclear excitations

are about eight orders of magnitude smaller than the elastic scattering cross section in the class of models we are interested in this paper. The reason is that in our models, deuteron dissociation can only be mediated by an isoscalar vector current, whereas in the Standard Model, the isovector axial vector gives by far the dominant contribution. Thus, considering the 4% uncertainty of the measurement [36] and the 16% uncertainty in the prediction based on the standard solar model [43], no deviations from the Standard Model are expected in SNO. Note, however, that a dedicated Borexino search for gamma ray lines from the process $^{12}\mathrm{C} + \nu \to \nu + {}^{12}\mathrm{C}^* \to \nu_b + {}^{12}\mathrm{C} + \gamma$ could be sensitive to the types of new physics discussed here [23]. Also, at much higher energies $\gtrsim 100$ MeV, there should be constraints from accelerator neutrino experiments such as MiniBooNE or MINOS. We see from figure 1b that in germanium solar neutrinos can only yield neutrino–nucleus scattering events with $E_r \lesssim 10$ keV because of the sharp drop-off of their spectrum at high energies. In materials containing lighter target nuclei, the upper end up the recoil spectrum can be higher, up to 20 keV for NaI and 30 keV for $CaWO_4$ [1]. Also, atmospheric neutrinos can induce scattering events with higher recoil energies [1], but because of their much lower flux, we ignore these events in this paper.

In the following sections, we will discuss how new contributions to neutrino–electron scattering and new contributions to neutrino–nucleus scattering can modify the event rates plotted in figure 1.

3. FOUR MODELS

We will now turn to new physics scenarios in which neutrino interactions with electrons and/or nuclei are enhanced to give event rates that are interesting for present and future dark matter direct detection experiments. As we have seen in the previous section, the precise measurements of the solar neutrino–electron scattering rate above few hundred keV in Borexino [34, 44, 45] and SNO [35, 36] set tight constraints on anomalous neutrino–electron interactions. Neutrino–nucleus interactions, on the other hand, should be constrained at energies $\gtrsim 100$ MeV by accelerator neutrino experiments. Thus, any new physics model that could potentially contribute significantly to the event rate in direct detection experiments should give a signal only at low recoil energies around a few keV, but die away at higher recoil energies.

The simplest possibility which fits the bill is a new interaction between neutrinos and electrons mediated by a very light or massless particle. In this case the matrix element for neutrino–electron or neutrino–nucleus scattering via the light particle contains a factor $q^{-2} = (2m_T E_r)^{-1}$, where q is the 4-momentum exchange, E_r is the electron recoil energy, and m_T is the mass of the target electron or nucleus. This will lead to a differential cross section which is a falling function of E_r. The new physics contribution can thus dominate the Standard Model rates at low energies relevant for direct detection, but not at high energies where neutrino detectors are sensitive.

3.1. Neutrino magnetic moments

Perhaps the phenomenologically simplest type of new physics leading to enhanced solar neutrino–electron scattering at low energies through the exchange of a light particle is a neutrino magnetic moment interaction of the form

$$\mathcal{L}_{\mu_\nu} \supset \mu_\nu \, \bar{\nu} \sigma^{\alpha\beta} \partial_\beta A_\alpha \nu \,, \tag{7}$$

where μ_ν is the neutrino magnetic moment and $\sigma^{\alpha\beta}$ is as usual defined in terms of the Dirac matrices as $\sigma^{\alpha\beta} = \frac{i}{2}[\gamma^\alpha, \gamma^\beta]$. In this case the light particle which mediates new interaction is the photon (A_α) itself. We included only dipole–charge interactions in equation (7), but we have

checked that dipole–dipole interactions are negligible compared to dipole–charge interactions at the recoil energies relevant to dark matter detectors, whereas at higher recoil energies, Standard Model weak interactions are dominant for all allowed values of μ_ν.

While the Standard Model prediction for the loop-induced neutrino magnetic moment, $\mu_\nu = 3.2 \times 10^{-19} \mu_B \times (m_\nu/\mathrm{eV})$ [46, 47] (with the Bohr magneton $\mu_B = \sqrt{4\pi\alpha}/2m_e$, α being the fine structure constant) is beyond the reach of current and near future experiments, some extensions of the Standard Model predict sizeable μ_ν [46, 48–52], potentially close to the current 90% CL upper limit $\mu_\nu < 0.32 \times 10^{-10} \mu_B$ from solar and reactor neutrino experiments [53], in particular GEMMA [42].[4] The differential neutrino–electron scattering rate through magnetic moment interactions is given by [59]

$$\frac{d\sigma_\mu(\nu e \to \nu e)}{dE_r} = \mu_\nu^2 \alpha \left(\frac{1}{E_r} - \frac{1}{E_\nu} \right), \tag{8}$$

and the corresponding expression for neutrino–nucleus scattering is

$$\frac{d\sigma_\mu(\nu N \to \nu N)}{dE_r} = \mu_\nu^2 \alpha Z^2 F^2(E_r) \left(\frac{1}{E_r} - \frac{1}{E_\nu} \right). \tag{9}$$

Here, Z is the nuclear charge, and $F(E_r)$ is the nuclear form factor (see discussion below equation (3)). Of course, ordinary scattering through W and Z exchange, with the cross section from equations (1)–(3) is also present. The dependence of equation (8) on the neutrino energy E_ν and the recoil energy E_r arises from the interplay of the photon propagator and the derivative in the magnetic moment interaction vertex, equation (7).

3.2. Gauged $B - L$

As we have seen in section 3.1, a magnetic moment contribution to the neutrino–electron and neutrino–nucleus scattering cross section falls proportional to E_r^{-1} at low recoil energy. We will now turn our attention to scattering processes for which the recoil energy spectrum falls even more steeply ($\propto E_r^{-2}$), and hence a larger enhancement of the neutrino scattering rate at low energies is possible without violating the Borexino constraint.

This can be achieved if there is a new neutrino–electron or neutrino–quark interaction mediated by a light particle whose couplings do not contain derivatives. Let us in particular consider a model with gauged $B-L$ (baryon number minus lepton number) symmetry, with the corresponding $U(1)_{B-L}$ gauge boson A' having a mass $M_{A'} \ll 1$ GeV:

$$\mathcal{L}_{B-L} \supset -g_{B-L}\, \bar{e}\gamma^\alpha A'_\alpha e + \frac{1}{3} g_{B-L}\, \bar{q}\gamma^\alpha A'_\alpha q - g_{B-L}\, \bar{\nu}\gamma^\alpha A'_\alpha \nu + \dots . \tag{10}$$

Here, g_{B-L} is the $U(1)_{B-L}$ coupling constant and q, e and ν are quark, charged lepton and neutrino fields, respectively. We will call A' a "dark photon" here and in the following.[5] Note that we neglect the possibility of kinetic mixing between the dark photon and the photon here. We will discuss models with kinetic mixing (but with couplings to $B - L$) in great detail below, and we will argue

[4] Published astrophysical constraints can be up to an order of magnitude stronger [53–58], but it is difficult to assess the systematic uncertainties associated with these limits and to assign a confidence level to them.

[5] In the literature, the term "dark photon" is often reserved for $U(1)'$ gauge bosons coupling to the Standard Model only through kinetic mixing with the photon, but we will use it in a more general context. In fact, a gauge boson coupled to Standard Model particles only through kinetic mixing with the photon, would not have tree level couplings to Standard Model neutrinos at all since they are electrically neutral.

in section 7 that, in many phenomenologically relevant processes, a coupling to $B-L$ is equivalent to kinetic mixing.

The cross section for A'-mediated elastic scattering of a neutrino off an electron or nucleus depends mildly on the chiral structure of the A' couplings. Here, for concreteness we will assume the A' to have pure vector couplings of the form $\bar{\psi}\gamma^\mu\psi_e\, A'_\mu$, but spectra would look similar for other chiral structures. With this assumption we obtain for the differential cross section for neutrino–electron scattering as a function of the recoil energy

$$\frac{d\sigma_{A'}(\nu e \to \nu e)}{dE_r} = \frac{g_{B-L}^4 m_e}{4\pi p_\nu^2 (M_{A'}^2 + 2E_r m_e)^2}\left[2E_\nu^2 + E_r^2 - 2E_r E_\nu - E_r m_e - m_\nu^2\right], \tag{11}$$

The corresponding expression for neutrino–nucleus scattering is straightforwardly obtained by replacing m_e with the nuclear mass, and by including a coherence factor A^2 (where A is the nuclear mass number) and the nuclear form factor $F^2(E_r)$.[6] Note that in equation (11) we do not neglect the neutrino mass m_ν and we distinguish between the neutrino energy E_ν and its momentum p_ν because later, in section 4, we will consider also scattering of heavy sterile neutrinos.

As we will expose in section 7, the parameter space for light $U(1)_{B-L}$ gauge bosons is strongly constrained by "fifth force" searches [60–63] which require a $U(1)_{B-L}$ gauge boson with couplings relevant to a dark matter detector to be heavier than about 100 eV. In addition, bounds on anomalous energy losses in stars and supernovae [64–66], as well as GEMMA limits on anomalous contributions to the scattering of reactor antineutrinos on electrons [42] severely limit the allowed range of coupling constants for 1 meV $\lesssim M_{A'} \lesssim$ 100 MeV. However, we will see that some interesting regions of parameter space are not yet fully excluded. Moreover, in slightly non-minimal models, many constraints can be easily avoided [20, 67].

3.3. Sterile neutrinos and a dark photon coupled through kinetic mixing

One simple possibility to avoid many constraints on light new gauge bosons while still maintaining large neutrino–electron and neutrino–nucleus scattering rates is to consider scenarios in which the couplings of the new gauge boson to electrons and other Standard Model particles are much smaller than its coupling to at least some neutrino flavors. This is possible in models with new sterile neutrinos, which are singlets under the Standard Model gauge group, but charged under a new $U(1)'$ gauge group. Standard Model particles, on the other hand, could be coupled to the A' gauge boson (which we again call the "dark photon") only through a small kinetic mixing ϵ with the photon. The relevant terms in the Lagrangian of the model below the electroweak scale are

$$\begin{aligned}\mathcal{L} \supset & -\frac{1}{4}F'_{\mu\nu}F'^{\mu\nu} - \frac{1}{4}F_{\mu\nu}F^{\mu\nu} - \frac{1}{2}\epsilon F'_{\mu\nu}F^{\mu\nu} + \bar{\nu}_s i\partial\!\!\!/\nu_s + g'\bar{\nu}_s\gamma^\mu\nu_s A'_\mu \\ & - \overline{(\nu_L)^c} m_{\nu_L}\nu_L - \overline{(\nu_s)^c} m_{\nu_s}\nu_s - \overline{(\nu_L)^c} m_{\rm mix}\nu_s\,,\end{aligned} \tag{12}$$

where the first line contains the gauge kinetic terms of the A' boson and the photon, the kinetic mixing term between A' and the photon with small mixing parameter ϵ, and the kinetic term of the sterile neutrino ν_s, including its gauge coupling to the A' with coupling constant g'. (We have omitted the kinetic terms of the other fermions and gauge bosons in the model since they are not relevant to our discussion and are anyway unchanged compared to the Standard Model.) We could equivalently have considered the interactions of A' above the electroweak scale, in which case

[6] For recoil energies below 10 keV, the inclusion of the form factor merely changes the count rate in a dark matter detector by 1–10%

the kinetic mixing would be between the dark photon and the hypercharge boson rather than the photon. This would introduce not only mixing between A' and A, but also mixing between A' and the Z, which is, however, negligible for the low energy processes we are interested in. The second line of equation (12) contains the usual 3×3 Majorana mass matrix for active neutrinos ν_L, a Majorana mass matrix for the sterile neutrinos, as well as a Majorana-type mixing term. These mass matrices may be obtained from a seesaw mechanism if we introduce singlet right-handed neutrinos ν_R:

$$-\bar{L} Y_\nu \tilde{H} \nu_R - \bar{\nu}_s Y_s H' \nu_R - \frac{1}{2} \overline{(\nu_R)^c} M_R \nu_R + h.c. \,, \tag{13}$$

where all fields are understood as vectors in flavor space: $\bar{L}$ contains the three Standard Model lepton doublets, ν_s contains n_s sterile neutrinos coupled to A', and ν_R contains $3+n_s$ heavy right-handed neutrinos. We use the notation H for the Standard Model Higgs boson, H' for a new Higgs boson which is charged under $U(1)'$ and breaks it when it acquires a vacuum expectation value (vev), and we define $\tilde{H} \equiv \epsilon^{ab} H_b^\dagger$, where ϵ^{ab} is the totally antisymmetric tensor in two dimensions and a, b are $SU(2)_L$ indices.[7] The Standard Model Yukawa coupling Y_ν, the Yukawa coupling of the sterile neutrinos Y_s, and the right-handed mass matrix M_R are understood to be matrices of size $3 \times (3+n_s)$, $n_s \times (3+n_s)$, and $(3+n_s) \times (3+n_s)$, respectively. According to the usual seesaw formula, the effective $(3+n_s) \times (3+n_s)$ Majorana mass matrix of the light neutrinos is given by

$$m_\nu = \begin{pmatrix} Y_\nu \langle H \rangle \\ Y_s \langle H' \rangle \end{pmatrix} M_R^{-1} \begin{pmatrix} Y_\nu \langle H \rangle \\ Y_s \langle H' \rangle \end{pmatrix}^T . \tag{14}$$

We have not explicitly written down the kinetic and potential terms for H and H', but we assume that they are such that H' acquires a small vev that gives the A' a mass consistent with the constraints from section 7, and the sterile neutrinos a mass that is sufficiently small to allow coherent mixing between active and sterile flavors at typical solar neutrino energies. Since the vev of H', denoted by $\langle H' \rangle$, is by assumption much smaller than the Standard Model Higgs vev $\langle H \rangle$, the mostly sterile neutrino mass eigenstate will typically be even lighter than the active ones unless there is a large hierarchy in the right-handed Majorana mass matrix M_R.

In models of the form (12), the sterile neutrino–electron scattering cross section is given by equation (11), with the replacement $g_{B-L} \to \sqrt{\epsilon e g'}$. Here, ϵe denotes the A' coupling to electrons, and g' denotes the $U(1)'$ gauge coupling constant. (If the dark photon is *very* light, so that the range of its interaction becomes macroscopic, there will be corrections to equation (11) at low recoil energy due to the breakdown of the one-boson-exchange approximation and due to possible shielding effects from a cosmic sterile neutrino background [68]. **CHECK THIS STATEMENT).** We will see that in such models, $d\sigma_{A'}(\nu e \to \nu e)/dE_r$ and $d\sigma_{A'}(\nu N \to \nu N)/dE_r$ can be significantly larger than in models with only the three active neutrinos.

A small admixture of sterile neutrinos to the solar neutrino flux can be produced by oscillation before the neutrinos reach the Earth. In a two-flavor approximation with only one active neutrino flavor ν_a and one sterile neutrino flavor ν_s, and with the corresponding mass eigenstates ν_2 and ν_4, the vacuum oscillation probability is given by the usual expression

$$P(\nu_a \to \nu_s) = \sin^2 2\theta_{24} \sin^2 \left(\frac{\Delta m_{42}^2 L}{4E} \right) , \tag{15}$$

where L is the distance traveled by the neutrinos, θ_{24} is the effective active–sterile neutrino mixing angle in vacuum, and $\Delta m_{42}^2 = m_4^2 - m_2^2$ is the splitting between the squared mass of the mostly

[7] We neglect the "Higgs portal" coupling $(H^\dagger H)(H'^\dagger H')$ here.

sterile mass eigenstate (m_4) and the mostly active mass eigenstate (m_2) in vacuum. The fraction of sterile flavors in the solar neutrino flux can be as large as 20–30% without violating SNO constraints on the rate of neutral current neutrino–nucleon interactions [69]. If the mass squared difference between active and sterile neutrinos is in the range $\Delta m^2_{41} \gtrsim 10^{-4}$ eV^2 accessible to terrestrial neutrino oscillation experiments, some of the active–sterile mixing angles are more strongly constrained, to the level of $\sin^2 2\theta \sim$ few % [8–10].

One potential problem with the model discussed here is that the sterile neutrinos (and also the hidden Higgs boson H' [70]) will acquire a tiny effective electromagnetic charge of order ϵ [71]. [8] There are tight limits on such "minicharged" particles, the strongest of which come from bounds on anomalous energy losses in stars due to the decay of plasmons into sterile neutrinos [65, 72].[9] Like bounds on dark photons, these constraints are also somewhat model dependent as we will discuss in section 7. For us, it is important to note that minicharged particles with sufficiently *large* coupling cannot leave a stellar environment and may therefore still be allowed. Also, models which raise the sterile neutrino mass to ~ 10 keV to several 100 keV (depending on ϵ) completely evade these limits.

Note that there are other constraints on sterile neutrinos with masses $\gtrsim 10$ KeV, the most severe of which come from observations of the x-ray flux from galaxy clusters and of the cosmic microwave background, see [73, 74]. These observables are modified if there is a large astrophysical population of sterile neutrinos decaying radiatively into light neutrinos. Other constraints could be derived from requiring the sterile neutrinos to not overclose the Universe. However, astrophysical and cosmological bounds can be avoided if sterile neutrinos are not produced in significant numbers in the early universe, for instance because of a low reheating temperature ($\ll 100$ MeV) [75], or because they are chameleon-like (i.e. their effective mass could depend on the surrounding matter density [20, 67, 76]). Alternatively, the sterile neutrinos could have a fast invisible decay mode, for instance into light neutrinos and Majorons [73].

The phenomenology of $\gtrsim 10$ keV sterile neutrinos in a direct detection experiment is essentially the same as that of the light sterile neutrinos discussed above, but their production in the Sun can be modified, especially due to kinematic suppression and because they can no longer interfere with the light active neutrinos. We discuss the construction of models with heavier sterile neutrinos in more detail in appendix A, and their interesting phenomenology in section 4.2.

3.4. Baryonic sterile neutrinos and gauged baryon number

While the models discussed so far are most easily detected in neutrino–electron scattering, it is phenomenologically interesting to consider also scenarios which predict neutrino–nucleus scattering to be dominant, in particular since nuclear recoils are the type of signal that most dark matter detectors are particularly sensitive to. A model of this type has been proposed in [23]: It extends the Standard Model by a gauged $U(1)_B$ (baryon number) symmetry and introduces one or several "baryonic" sterile neutrinos which are charged under $U(1)_B$. Since constraints on new light gauge bosons coupling to quarks are much weaker than constraints on particles coupling to leptons (see

[8] This is true in a basis where the kinetic mixing term has been transformed away by the replacement $A'_\mu \to A'_\mu - \epsilon A_\mu$ and the mass matrix of the two $U(1)$ gauge bosons is hence off-diagonal. In parts of the literature, a basis with a diagonal mass matrix is used, in which case no electromagnetic minicharges occur. Of course, the constraints discussed here are basis-independent.

[9] Plasmon oscillations and plasmon decay into sterile neutrinos is also an alternative production mechanism for sterile neutrinos in the Sun. However, the A' spectrum and hence also the sterile neutrino spectrum in this case are determined by thermal effects and are steeply falling functions of energy above 1 keV [64]. We have checked that therefore the flux at energies accessible to dark matter experiments is negligibly small.

section 7 below), the $U(1)_B$ gauge coupling can be fairly large.

The cross section for sterile neutrino–nucleus scattering in this model is given by equation (11), with g_{B-L} replaced by the $U(1)_B$ gauge coupling g_B, and with the usual coherence factor A^2 and the nuclear form factor $F^2(E_r)$ included.

In addition to enhancing neutrino scattering cross sections, a $U(1)_B$ gauge boson is also a source of new Mikheyev-Smirnov-Wolfenstein (MSW) type neutrino matter effects [77, 78]. In particular, A'-mediated coherent forward scattering of sterile neutrinos on nucleons creates a potential of the form

$$V_{A'} = \frac{g_B^2}{M_{A'}^2} \left(N_p + N_n\right) \tag{16}$$

where N_p and N_n are the proton and neutron number densities in the Sun, respectively, which are a function of the distance from the center [43]. Note that this form of the MSW potential is specific to the $U(1)_B$ model. The $U(1)'$ model discussed in section 3.3, for instance, does *not* lead to non-standard matter effects at all because the couplings of a kinetically mixed $U(1)'$ gauge boson are proportional to electric charge, which is zero for ordinary matter, whereas a $U(1)_{B-L}$ model leads to a potential proportional to the number density of neutrons. (In the $U(1)_{B-L}$ model from section 3.2, this matter potential is however inconsequential for oscillation physics since it is flavor-diagonal among the active neutrinos.)

The phenomenological implications of the new MSW potential are twofold: On the one hand, in the large potential limit

$$V_{A'} \gg \max_{j,k} |\Delta m_{jk}^2|/2E\,, \qquad\qquad j,\, k = 1 \ldots \text{number of neutrino mass eigenstates}\,, \tag{17}$$

the Hamiltonian terms mixing active and sterile neutrinos are negligible compared to the large potential term for the sterile neutrinos. (Here, E is the neutrino energy, which is $\gtrsim 10$ MeV for the neutrinos of interest to dark matter detectors.) Thus, in this case, the effective active–sterile mixing angles in matter are very small, and sterile neutrinos are effectively decoupled in matter. Their production in the Sun is then negligible, and they are only produced via vacuum oscillations outside the Sun.

On the other hand, even when active–sterile oscillations are suppressed, the existence of the $V_{A'}$ term can still modify oscillations among the three active neutrino flavors. For each parameter point considered, one needs to check that the agreement of the theory with data from solar, atmospheric, reactor, and accelerator neutrino experiments is not spoiled. For solar neutrinos, this requires checking that the $\nu_e \to \nu_e$ survival probability between $\sim$ 200 keV–20 MeV is not modified substantially compared to the standard three-flavor case. Since in some models, Earth matter effects can lead to different survival probabilities during daytime and nighttime, one should also make sure that no such day–night asymmetry is present. For terrestrial neutrinos, one has to check that the $\overset{(-)}{\nu}_e \to \overset{(-)}{\nu}_e$ and $\overset{(-)}{\nu}_\mu \to \overset{(-)}{\nu}_\mu$ survival probabilities, as well as the $\overset{(-)}{\nu}_\mu \leftrightarrow \overset{(-)}{\nu}_e$ and $\overset{(-)}{\nu}_\mu \to \overset{(-)}{\nu}_\tau$ oscillation probabilities are not modified substantially.

Finally, the existence of a non-standard matter potential could imply the existence of new MSW resonances which may lead to strong conversion of active neutrinos into sterile states. These MSW resonances can usually be avoided by choosing an appropriate sign for the active–sterile mass differences.

4. ENHANCED NEUTRINO–ELECTRON SCATTERING FROM NEW PHYSICS

Let us now investigate the phenomenology of the models introduced in section 3 in more detail. We begin by studying neutrino–electron scattering rates in dark matter detectors. Most of these

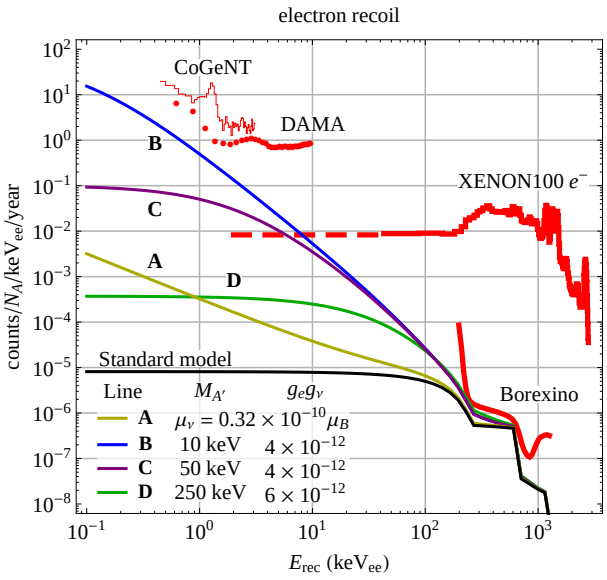

Figure 2: Expected event spectra in a dark matter detector from new physics in the scattering of solar neutrinos on electrons. The different colored curves correspond to (A) a model where the neutrino has a magnetic dipole moment of $\mu_\nu = 0.32 \times 10^{-10} \mu_B$ and (B, C, D) models where the scattering is enhanced by the exchange of a new light gauge boson A' with couplings g_e to electrons and g_ν to neutrinos. The latter case is for instance realized in the model from section 3.3, where Standard Model particles couple to the A' through its kinetic mixing with the photon, but there is also a sterile neutrino ν_s directly charged under $U(1)'$. To keep the discussion general, we assume the $\nu_e \to \nu_s$ transition probability to be energy-independent, and we have absorbed the corresponding flux suppression into a redefinition of g_ν^2. The black curve shows the Standard Model rate from figure 1, and the red curves and data points show the observed electron recoil rates in XENON-100 [39] (see section 2 for details), Borexino [34], CoGeNT [25], and DAMA [40]. (Note that CoGeNT and DAMA cannot distinguish nuclear recoils from electron recoils, so their data can be interpreted as either.)

experiments make an effort to distinguish nuclear and electron recoils, focusing on the former as dark matter candidate events and rejecting the latter as backgrounds. Interestingly, two exceptions to this are DAMA [40] and CoGeNT [24], both of which have observed a possible signal. We will begin with scenarios in which the scattering neutrinos (either active or sterile) are light ($\lesssim 1$ eV), and later consider also heavier sterile neutrinos.

4.1. Scattering of Light Neutrinos

Curve A in figure 2 shows the neutrino–electron scattering rate expected for neutrinos with a magnetic moment (section 3.1) of $0.32 \times 10^{-10} \mu_B$, saturating the 90% C.L. limit from the GEMMA experiment [42]. We see that a significant enhancement of the event rate, by more than one order of magnitude at $E_r \sim$ few keV, is possible. While this is still outside the reach of existing experiments, near future detectors like LUX, XENON-1T, X-MASS or PANDA-X may be able to enter this territory because the self-shielding capabilities of large liquid noble gas detectors are expected to lead to a significant reduction in radioactive background levels. Once the uncertainty on the background rate drops below the expected signal rate, future dark matter detectors may be able to improve the bounds on the magnetic dipole moment of the neutrino considerably.

Curves B, C and D in figure 2 are typical event spectra from A'-mediated neutrino–electron

scattering in a dark matter detector. We see that, as expected, the electron recoil energy spectrum is proportional to the squared propagator of the light gauge boson, $(q^2 - M_{A'}^2)^{-2}$ where $q^2 = -2E_r m_e$. It is thus a steeply falling function of E_r for $E_r > M_{A'}^2/2m_e$ and flattens out for lower E_r. This can be easily discerned by comparing curves B, C and D, which where computed assuming different values for $M_{A'}$. All three of these curves satisfy (but almost saturate) the Borexino limit, and all of them may be within the reach of LUX, XENON-1T, X-MASS, PANDA-X or even XENON-100, provided the detector response to electron recoils can be sufficiently well understood, and the electron recoil background from Standard Model processes can be sufficiently reduced. Even now, XENON-100 disfavors scenarios in which *all* of the events seen in CoGeNT or DAMA are explained by the scattering of solar neutrinos on electrons. It is of course still conceivable that only a fraction of these rates signifies the scattering of sterile neutrinos on electrons, and the rest is due to instrumental backgrounds. In fact, a recent preliminary investigation by the CoGeNT collaboration [79] suggests that such instrumental backgrounds exist. The annual modulation amplitudes observed by DAMA and CoGeNT are roughly at the level of the XENON-100 background, and we may hope to explain these signals in models that predict a strongly modulating signal, see section 6.

Curves B, C and D in figure 2 were computed with the $U(1)_{B-L}$ model from section 3.2 and the $U(1)'$ model with kinetic mixing and $U(1)'$-charged sterile neutrinos from section 3.3 in mind. The former model is more strongly constrained since it predicts enhanced scattering rates of even the active neutrinos at low energies. Such signals are constrained by low-energy neutrino–electron scattering experiments at nuclear reactors, in particular GEMMA [42], and they may also be in conflict with constraints on any anomalous energy loss in the Sun and in other stars. (see section 7). Astrophysical constraints can often be avoided in "chameleon" models, where the dark photon mass depends on the background matter density [20, 67, 76].

The $U(1)'$ model with kinetic mixing allows for much more model-building freedom than the $U(1)_{B-L}$ model as long as it is ensured that the oscillation lengths for transitions of active neutrinos into the more strongly interacting sterile neutrinos,

$$L_{\text{osc}} = \frac{4\pi E}{\Delta m_{4i}^2} \simeq 2.48 \text{ km} \times \left(\frac{E}{\text{MeV}}\right)\left(\frac{\text{eV}^2}{\Delta m_{4i}^2}\right), \qquad (i = 1, 2, 3)\,, \tag{18}$$

are much longer than the distance of the GEMMA detector from the reactor core (13.9 m [42]). Here, we have assumed that this is the case, but that at the same time

$$L_{\text{osc}} \ll 1 \text{ AU} \tag{19}$$

in the neutrino energy range relevant to dark matter detectors, 10 keV $\lesssim E_\nu \lesssim$ 15 MeV, so that the L-independent oscillatory term in equation (15) averages to 1/2 and the fraction of solar neutrinos converted into sterile states, $P(\nu_e \to \nu_s)$, is energy-independent. Condition (19) is fulfilled for $\Delta m_{4i}^2 \gg 2.5 \times 10^{-10}$ eV^2 $(i = 1, 2, 3)$. To avoid astrophysical constraints on kinetically mixed $U(1)'$ gauge bosons and on sterile neutrinos more easily, one can (but does not have to, see section 7) consider sterile neutrinos heavier than ~ 10 keV or chameleon models [20, 67, 76].

Note that in the $U(1)'$ model with kinetic mixing (or in any model where the signals shown in figure 2 originate from the scattering of sterile neutrinos), the product of couplings $g_\nu g_e$ needed to obtain the displayed curves needs to be larger in order to compensate for the mixing angle-suppressed flux. This is, however, easily achieved by increasing the coupling of dark photons to sterile neutrinos while leaving the coupling to electrons small, or even reducing it compared to the $U(1)_{B-L}$ case. In the legend of figure 2 it is understood that in models where the enhanced event rate is due to sterile neutrinos, the fraction of solar neutrinos converted into sterile states, $P(\nu_e \to \nu_s)$, is absorbed into a redefinition of g_ν^2.

4.2. Heavy Sterile Neutrinos

In the scenarios shown in figure 2, the electron recoil spectra in the few–10 keV region were falling at most as E_r^{-2}, so that a scattering rate larger than the one shown in curve B is excluded by Borexino, and possibly also by XENON-100 constraints. However, we note that the recoil spectrum has several sharp edges at higher energies of several hundred keV or above. These features are induced by the kinematic cutoffs of the individual processes contributing to the solar neutrino flux (see figure 1 for a break-down of the recoil spectrum into these contributions). We will now show how these kinematic edges can be shifted down to the recoil energies of interest to dark matter detectors. This can happen in models with heavy sterile neutrinos whose mass is close to one of the kinematic edges in the solar neutrino flux. Here, we will in particular focus on the sharpest of these edges, coming from neutrinos produced in the reaction

$$^7\mathrm{Be} + e^- \to {}^7\mathrm{Li} + \nu_i \,, \tag{20}$$

with an energy of 862 keV.

For sterile neutrinos with a mass of that order, the velocity difference between the heavy and light states produced in the Sun is so large that the neutrino flux can be viewed as a completely incoherent mixture of heavy and light states. Hence, dynamic transitions between the active and sterile flavor eigenstates during propagation are absent. (There can still be coherence among the light states and among the heavy states, provided the mass splittings within each of the two sectors are sufficiently small.) We will assume that the electron recoil signal is dominated by sterile neutrino scattering, as is the case for instance in the $U(1)'$ model from section 3.3. We will also assume that the sterile flavor admixture to the light mass eigenstates is negligible, whereas there needs to be some admixture of the heavy mass eigenstate ν_4 to the active flavor eigenstates in order to produce ν_4 in the Sun. See Appendix A for a discussion of models in which this is naturally achieved.

Examples for the expected electron recoil rates from scattering of heavy sterile neutrinos with a mass not far below the ^{7}Be line are shown in figure 3. Even though production of the heavy mass eigenstate ν_4 in the reaction (20) is suppressed by the small mixing matrix element $|U_{e4}|^2$ and by kinematic factors which are small for ν_4 masses close to the Q value of the production reaction, a considerable enhancement of the neutrino–electron scattering rate in dark matter experiments is still possible. Note that in the plot we have not taken into account kinematic modifications to solar neutrino production processes other than (20), many of which have 3-body final states. Instead, we have simply assumed the ν_4 produced in these reactions to have the same energy spectrum (suppressed only by the small leptonic mixing matrix element $|U_{e4}|^2$) as the corresponding light neutrinos. This introduces inaccuracies close to the upper kinematic thresholds of the pp, ^{13}N, ^{15}O, ^{17}F, ^{8}B and hep neutrino spectra, and to remind the reader of these inaccuracies we show the corresponding contributions to neutrino–electron scattering as dashed lines in figure 3.

The plot shows that a model with heavy sterile neutrinos can explain an excess in low-threshold experiments like CoGeNT, while avoiding constraints from higher-energy detectors such as XENON-100 and Borexino. A certain amount of fine-tuning is, however, required in the particular case of CoGeNT since the CoGeNT and XENON-100 thresholds are relatively close to each other. Such tuning of a mass splitting against an unrelated quantity (the ^{7}Be line energy in this case) is reminiscent of tunings of the mass splitting against the dark matter kinetic energy in models of inelastic dark matter [80, 81], which were also introduced to reduce tensions among direct detection experiments.

The allowed masses and mixing angles of sterile neutrinos are constrained by a large number of terrestrial and astrophysical experiments, as explained at the end of section 3.3, but as also discussed there, these constraints can be avoided in slightly non-minimal scenarios.

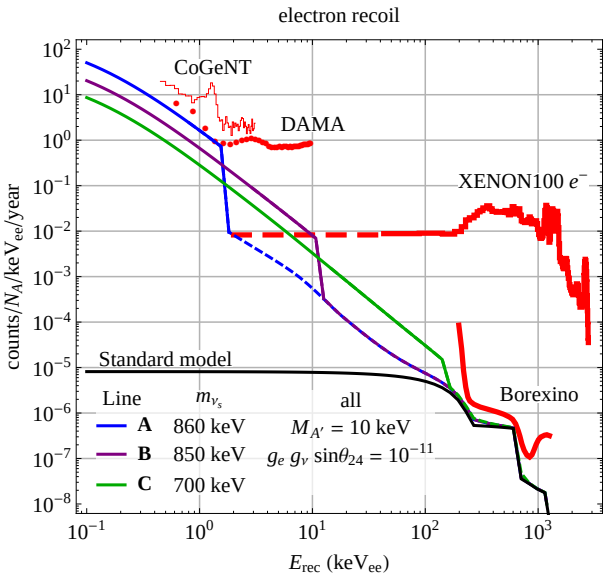

Figure 3: Expected event spectra in a dark matter detector from A'-enhanced scattering of heavy sterile neutrinos on electrons (thick colored lines, see figure legend for the parameters used). We have assumed the A' mass to be almost negligible, and we have chosen the cross section such that the CoGeNT excess can be explained. Black lines show the count rate in the Standard Model, and red curves show the observed event rates in XENON-100 [39] (see section 2 for details), Borexino [34], CoGeNT [25] and DAMA [40]. We have accounted for the kinematic suppression of heavy neutrino production for the ^{7}Be neutrinos (solid colored lines), but not of the pp, ^{13}N, ^{15}O, ^{17}F, ^{8}B and hep neutrinos (dashed colored line), which are produced as parts of 3-body final states.

5. ENHANCED NEUTRINO–NUCLEUS SCATTERING FROM NEW PHYSICS

While neutrino–electron scattering in a dark matter detector, as discussed in the previous section, is a very interesting discovery channel for new physics in the neutrino sector, it is not the process that most of these detectors are designed to look for. Let us therefore now turn our attention to neutrino–nucleus scattering, focusing in particular on scenarios in which the scattering rate at low energies is enhanced, thus possibly mimicking a dark matter signal.

As for neutrino–electron scattering, the simplest way of achieving such enhancement is by introducing a neutrino magnetic moment. The expected neutrino–nucleus scattering rate for solar neutrinos with a magnetic moment at the current upper limit is shown in figure 4, curve A, for four different target materials: germanium (used for instance in CoGeNT and CDMS), $CaWO_4$ (used in CRESST), NaI(Tl) (used for instance in DAMA), and xenon (used for instance in XENON-100, LUX, X-MASS, ZEPLIN, PANDA-X). As we can see, the effect is very small, and certainly not detectable by dark matter experiments in the foreseeable future.

The situation is different for neutrino–nucleus scattering through the exchange of a new light gauge boson ("dark photon") A' with mass $M_{A'}$ (see for instance the models from sections 3.2–3.4). In this case, the A' couplings can still be sufficiently large to allow for substantial enhancement of the scattering rate. Moreover, when scattering on a heavy nucleus, a low energy neutrino cannot resolve the nuclear substructure, and hence the scattering happens coherently on all nucleons. This leads to an increase in the cross section proportional to the nuclear mass number A.

On the other hand, since nuclei are much heavier than electrons, an $\mathcal{O}$(keV) nuclear recoil energy (above the detection threshold in a dark matter detector) requires neutrino energies of

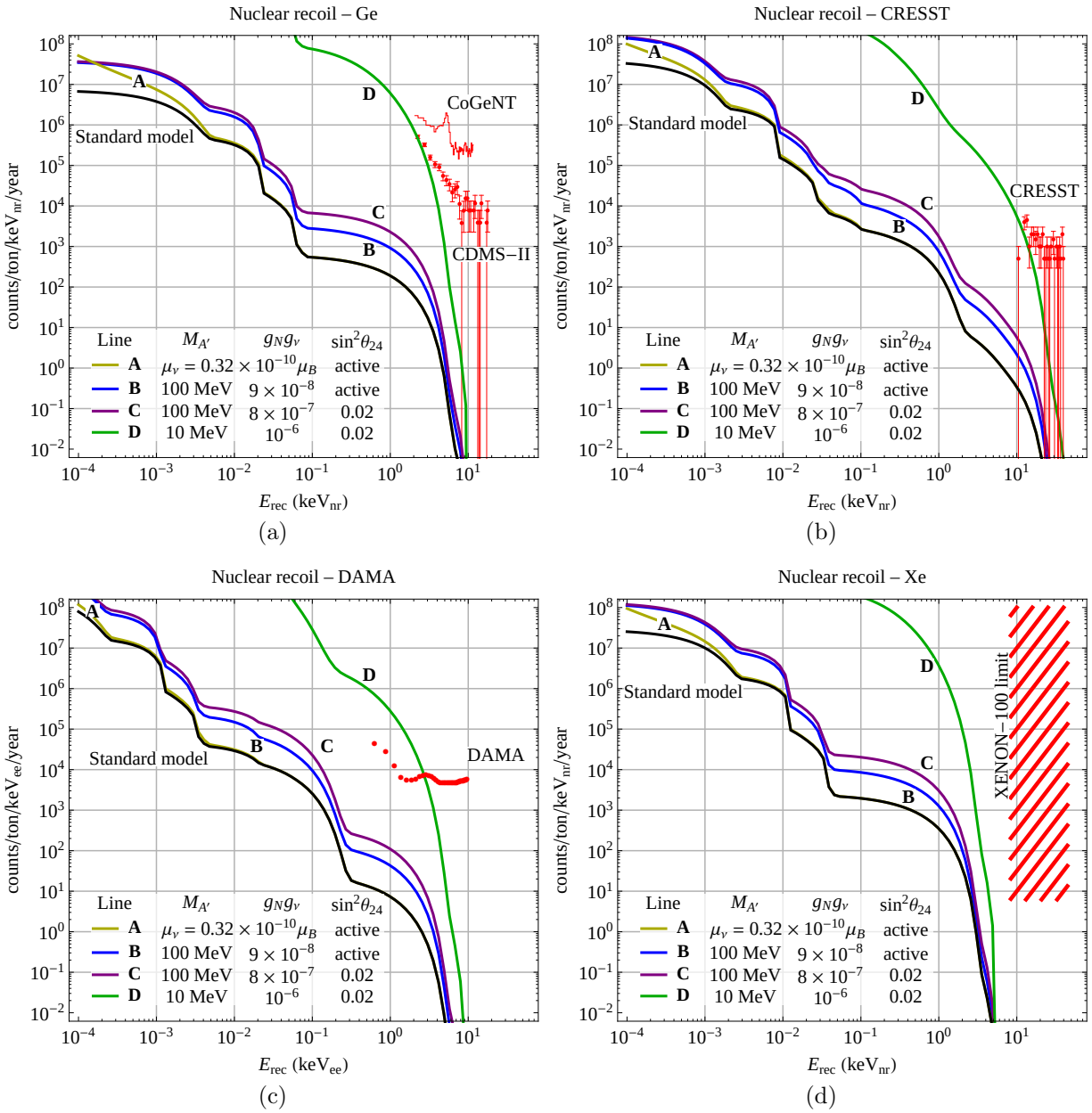

Figure 4: Expected event spectra in dark matter detectors from solar neutrino–nucleus scattering in (a) germanium, (b) $CaWO_4$, (c) NaI(Tl), and (d) xenon. Note that for NaI(Tl), we use units of keVee rather than keVnr for E_r because due to the different quenching factors for Na (0.3) and I (0.09) [82], the nuclear recoil energy cannot be uniquely reconstructed. Colored curves correspond to (A) a scenario with a neutrino magnetic moment $\mu_\nu = 0.32 \times 10^{-10}\mu_B$, (B) a model with active neutrino–nucleus scattering through a light A' boson (for instance the $U(1)_{B-L}$ model from section 3.2), and (C), (D) a model in which 2% of the solar neutrino flux oscillate into a Standard Model singlet ν_s, which couples to atomic nuclei for instance via a light $U(1)_B$ gauge boson (section 3.4) [23]. The relevant model parameters, in particular the mass of the A' and its coupling to nucleons ($g_p = g_n \equiv g_N$) are listed in the legend. Where applicable, we have assumed active–sterile mixing with $\sin^2\theta_{24} = 0.02$ and $\Delta m^2_{42} = 10^{-10}$ eV^2. The black curves show the Standard Model rate, and the red curves and data points show the observed spectra of nuclear recoil candidates in CoGeNT [25], in the low-threshold data set from CDMS [32], in CRESST [26], and in DAMA [40]. The approximate Xenon-100 exclusion region is obtained by converting Xenon-100's observed rate of signal candidates (3 events/100.9 days/48 kg between 8.4 keVnr and 44.6 keVnr [83]) into the units of our plots.

$\mathcal{O}$(1–10 MeV), as opposed to the $\mathcal{O}$(10 keV) required for the a detectable electron recoil. This means that, while all solar neutrino flux components can contribute to ν–e$^-$ scattering, only the ^{8}B and hep neutrinos—the components with the highest energy cutoff and the smallest flux—can affect the nuclear recoil signal. This leads to a reduction of 3 or 4 orders of magnitude when compared to the ^{7}Be and pp fluxes, respectively.

Moreover, the typical 4-momentum exchange $q^2 = -2E_r m_N$ in neutrino–nucleus scattering is much larger than in a neutrino–electron scattering process with the same recoil energy E_r. Therefore in order to obtain substantial count rates, much higher couplings are needed in comparison to the ν–e$^-$ scenarios considered before. Also, the larger q^2 means that the transition between flat and decreasing $d\sigma/dE_r$ happens at much larger $M_{A'}$.

In figure 4 (curves B–D), we plot the A'-mediated neutrino–nucleus scattering rate for three different scenarios. The first one, curve B, involves only the three active neutrinos, assuming that they couple universally both to electrons and nucleons. This scenario could, for instance, be realized in the $U(1)_{B-L}$ model from section 3.2. To obtain a sizeable count rate in nuclear recoils, and not violate the Borexino constraint on neutrino–electron scattering, we need an A' mass heavy enough to suppress ν–e$^-$ scattering, but not too heavy so that low energy neutrino–nucleus scattering is still enhanced. Curve B in figure 4 is a possible realization of this scenario which avoids all bounds to date (see discussion in section 7 and figure 8). We see that, although the nuclear recoil rate in this model is higher than the Standard Model rates, it is still at least 2–3 orders of magnitude lower than the sensitivity of CoGeNT, CDMS, CRESST or DAMA, thus making it difficult to probe in present and near future experiments.

Another possibility is to introduce sterile neutrinos which couple only to quarks, but not to leptons, as is the case for instance in a model with gauged baryon number and with sterile neutrinos charged under it (see [23] and section 3.4). Since the active neutrinos would not feel the new interaction, matter effects between the active and sterile sectors would arise. Hence, oscillation physics should be taken into account when computing the sterile neutrino flux at the Earth because, in principle, it could play an important role in such a scenario. To illustrate the impact of oscillations, we plot curve C in figure 4, for which we have assumed $\Delta m^2_{42} = 10^{-10}$ eV^2, and we have chosen the couplings $g_\nu g_N$ such that the predicted event rates are comparable to the ones for the $U(1)_{B-L}$ model, curve B.[10] Comparing curves B and C, we see that matter effects in this particular model change the rates moderately, but in an energy-dependent way. We have checked that oscillations of active neutrinos in solar and terrestrial scenarios are unaffected for our choice of parameters.

Note that curve C could also be realized in the model from section 3.3, with a gauge group $U(1)'$ under which only the sterile neutrinos are charged, and which couples to the Standard Model through kinetic mixing with the photon. An advantage of the $U(1)_B$ scenario is that Borexino limits, as well as bounds from fixed target experiments, atomic physics, and the anomalous magnetic moment of the muon and the electron (see section 7) can be more easily avoided, thus opening up a generous window in the parameter space for mediator masses from MeV to GeV and reasonably large couplings. The lack of strong limits makes it even possible to have rates high enough to explain the current signals in CoGeNT, CRESST and DAMA. However, since only the most energetic ^{8}B neutrinos can lead to nuclear recoils above threshold in these detectors, and since the neutrino spectrum is steeply decreasing with energy, the event spectra cannot be fitted very well, as can be seen in curve D in figure 4. For this curve, we have again assumed $\Delta m^2_{42} \approx 10^{-10}$ eV^2.

[10] Our choice of the mass squared difference allows to have annual modulation compatible with DAMA or CoGeNT, see section 6.2.

6. ANNUAL AND DIURNAL MODULATION

A generic prediction of almost all dark matter models is an annual modulation of the dark matter interaction rate observed at the Earth. This modulation is caused by the relative velocity of the Earth with respect to the Milky Way's dark matter halo, which is larger in northern hemisphere summer than in winter. In fact, the DAMA collaboration has reported a statistically significant annual modulation in the observed event rate [27, 40] (see, however, [84–88] for a discussion of systematic effects that could cause this modulation). Recently, the CoGeNT collaboration has also claimed a modulating signal [25], but its statistical significance is still lower and an interpretation in terms of dark matter is problematic [89–92] (see, however, [93, 94] which come to different conclusions). Both DAMA and CoGeNT observe the maximum count rate during the northern hemisphere summer or spring months (early June for DAMA and mid-April for CoGeNT). Other experiments have not yet published searches for annual modulation, but once an experiment has collected a sufficient number of candidate events, such a search would be the logical next step. Another potential "smoking gun" signature of dark matter is diurnal modulation, caused by the changes in relative velocity between the detector and the dark matter halo during the day. This modulation is predicted to be much smaller than the annual one, but it is nevertheless being searched for [92, 95], though with negative results so far. A significant improvement in the sensitivity to daily modulation is expected in dark matter detectors with directional sensitivity [96].

Because of the DAMA and CoGeNT signals, but also to scrutinize the robustness of the dark matter interpretation of *any* annual or diurnal modulation signal in the future, it is important to investigate alternative sources of temporal modulation in a dark matter detector. In this section we investigate modulation signals that could arise from neutrino physics beyond the Standard Model, and we discuss if and how these signals can be distinguished from a dark matter signal.

6.1. The Earth–Sun distance

Any signal whose source is an isotropic particle flux from the Sun is expected to show annual modulation due to the fact that the flux decreases with the square of the Earth–Sun distance, and that the Earth's orbit is slightly elliptical. At its closest point, the perihelion, around January 3rd, the Earth–Sun distance is 0.983 AU, versus 1.017 AU at the aphelion around July 4th. Hence, a solar neutrino signal will be modulated with an amplitude of about 3%, with the maximum count rate expected in early January. The expected phase would thus be *opposite* to the one observed in DAMA, but it is important to note that, depending on the dark matter mass and velocity distribution, dark matter can also lead to modulating signals peaking in winter [97]. Thus, a neutrino signal modulating predominantly because of the ellipticity of the Earth's orbit cannot explain the DAMA signal, but could be confused with other dark matter signals.

In the following, we will see that there may be additional sources of modulation that can potentially be large enough to overcompensate the Earth–Sun distance effect and thus reverse the sign of the modulation, bringing it in line with the DAMA observation.

6.2. Annual modulation from neutrino oscillations in vacuum

A simple way of overcompensating for the Earth–Sun distance effect is to assume that the anomalous signal we are interested in is exclusively due to new light sterile neutrinos (see e.g. the $U(1)'$ model from section 3.3 or the $U(1)_B$ model from section 3.4), and that these sterile neutrinos mix with the active neutrinos in such a way that the oscillation probability is increasing with increasing Earth–Sun distance. Then, oscillations would modify the simple L^{-2} scaling of

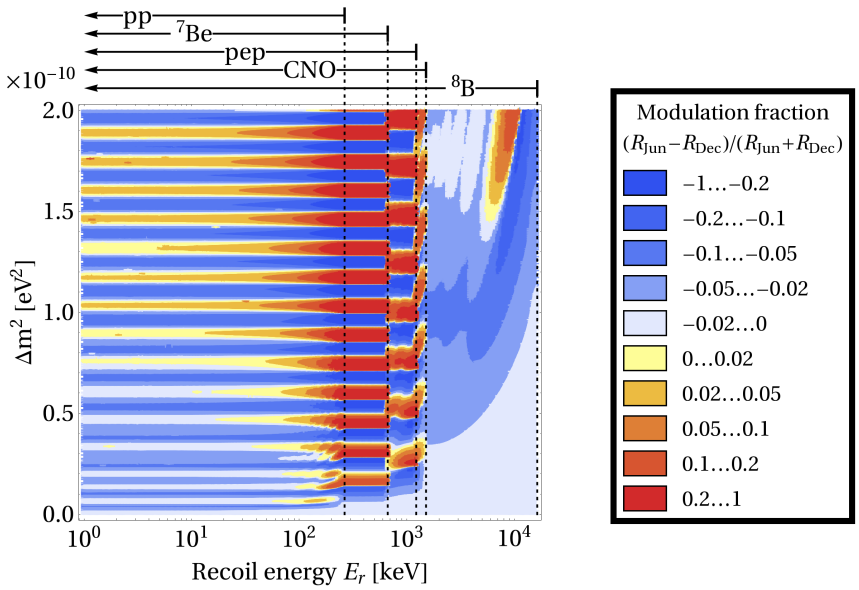

Figure 5: Relative annual modulation fraction $(R_{\rm Jun}-R_{\rm Dec})/(R_{\rm Jun}+R_{\rm Dec})$ of the rate of A'-mediated sterile neutrino–electron scattering as a function of the recoil energy E_r and the mass squared difference between active and sterile neutrinos. For simplicity, we use a two-flavor vacuum oscillation framework here. One can clearly distinguish five different regimes, in which the rate is dominated by pp neutrinos, ^{7}Be neutrinos, pep neutrinos, CNO neutrinos, and ^{8}B neutrinos, respectively.

the sterile neutrino flux with distance L, and in particular the sign of the modulation can be reversed [23]. This is illustrated in figure 5, where we plot the expected relative annual modulation amplitude, $(R_{\rm Jun} - R_{\rm Dec})/(R_{\rm Jun} + R_{\rm Dec})$ for sterile neutrino–electron scattering as a function of the electron recoil energy E_r and the mass squared difference Δm^2 between the mostly active and mostly sterile mass eigenstates. (Here, R stands for the count rate differential in E_r, and the subscripts "Jun" and "Dec" indicate the count rate at the northern hemisphere summer and winter solstice, respectively.) Note that, in producing figure 5, we have worked in a simple two-flavor oscillation framework, a situation which could be realized in a 4-neutrino model, where the mostly sterile mass eigenstate ν_4 mixes predominantly with only one of the active mass eigenstates, say ν_2. We have moreover assumed that the conversion of active neutrinos into sterile neutrinos proceeds through vacuum oscillations. This is realized for instance in the $U(1)'$ model with kinetic mixing from section 3.3, in which no non-standard matter effects arise due to the zero net electric charge of the Sun. In models where the two-flavor/vacuum approximation is not justified, the phenomenology could be much richer and much more complicated.

We see from figure 5 that a sizeable annual modulation fraction can be achieved without undue fine-tuning of Δm^2 *if* the oscillation length $L_{\rm osc} = 4\pi E_\nu/\Delta m^2$ at the relevant neutrino energies between few $\times$ 10 keV and $\sim$ 15 MeV is smaller but still comparable to the Earth–Sun distance. Such a situation would be reminiscent of the now excluded "just-so" solution to the solar neutrino problem, where it was also hypothesized that the oscillation length of solar neutrinos could be comparable to 1 AU. It is easy to distinguish four different energy regimes in figure 5, in which the scattering rate is dominated by pp neutrinos, ^{7}Be neutrinos, pep neutrinos, CNO neutrinos, and ^{8}B neutrinos, respectively. In each of these regimes, the modulation fraction is determined mostly by the oscillation length at the peak energy of the corresponding neutrino flux, as long as the recoil

energy is large enough for this peak energy to be kinematically accessible.

Note that for Δm^2 values larger than the ones shown in figure 5, the impact of oscillations will fade away once the oscillation length at the relevant neutrino energies becomes smaller than the diameter of the neutrino production region in the Sun. For pp neutrinos, which are produced at radii $r < 0.2 R_\odot$ in the Sun and whose flux peaks at around 300 keV, this happens for $\Delta m^2 \gtrsim 3 \times 10^{-9}$ eV^2, whereas for ^{8}B neutrinos, which are produced at $r < 0.1 R_\odot$ and whose flux peaks at around 6 MeV, wash-out effects become relevant only for $\Delta m^2 \gtrsim 10^{-7}$ eV^2 [98].

Note also that for $\Delta m^2 \sim 10^{-10}$ eV^2, the Standard Model MSW potential (or the A'-induced matter potential in the case of the $U(1)_B$ models from section 3.4) will suppress the mixing of electron neutrinos with sterile neutrinos at the center of the Sun. As the neutrinos propagate out, they can pass through an MSW resonance (if Δm^2 has the appropriate sign) and acquire an admixture of the mostly sterile mass eigenstate ν_4 because the resonance transition is non-adibatic, for such small Δm^2. (This can be seen from equation (23) below.)

6.3. Diurnal and annual modulation from Earth matter effects

Another mechanism by which solar neutrino signals can modulate with time is Mikheyev-Smirnov-Wolfenstein (MSW) type matter effects in the Earth. It is well known (see for instance reference [99] and references therein) that even in the standard three-flavor oscillation framework matter-enhanced $\nu_\mu, \nu_\tau \to \nu_e$ oscillations of solar neutrinos inside the Earth can lead to a slightly enhanced ν_e flux during the night, when solar neutrinos have to traverse the Earth before reaching a detector. This leads to diurnal modulation of the ν_e detection rate, and, since nights are longer in winter than in summer, it also leads to annual modulation. In the standard framework, the day–night asymmetry is predicted to be very small, on the few per cent level, but we will argue here that it can be sizeable in the new physics sector.

Consider, for instance, a scenario based on the model from section 3.4 (a $U(1)_B$ gauge boson), but with *two* sterile neutrinos, weakly mixed with the active ones. We assume that one of the sterile neutrino flavors, say ν_{s1}, is charged under the new gauge group, whereas the other, ν_{s2}, is not. Thus, only ν_{s1} can be observed in a detector. To simplify the discussion, we also assume both of the mostly sterile mass eigenstates to be heavy enough for them to be never produced in coherent superposition with the mostly active mass eigenstates, so that oscillations among the active flavors are fully decoupled from oscillations among the sterile flavors. We do, however, assume the mass splitting Δm^2 between the sterile neutrinos to be sufficiently small for oscillations among them to occur. We can then discuss these oscillations in a simple two-flavor framework.

Using the well-known formalism of neutrino oscillations in matter, it is straightforward to show that the probability for a solar neutrino to arrive in a terrestrial detector in the ν_{s1} flavor eigenstate is given by (see appendix) [99]

$$P(\nu_e \to \nu_{s1}) = |U^\odot_{e4}|^2 \cos^2\theta + |U^\odot_{e5}|^2 \sin^2\theta + (|U^\odot_{e5}|^2 - |U^\odot_{e4}|^2) \sin^2 2\theta \frac{2EV^\oplus_{A'}}{\omega^2 \Delta m^2} \sin^2 \frac{\omega \Delta m^2 L^\oplus}{4E} \,. \quad (21)$$

Here, $U^\odot_{e4}$ and $U^\odot_{e5}$ are elements of the effective leptonic mixing matrix in matter at the core of the Sun, θ is the vacuum mixing angle between ν_{s1} and ν_{s2}, E is the neutrino energy, $L^\oplus$ is the distance the neutrinos travel inside the Earth, and $V^\oplus_{A'}$ is the A'-mediated MSW matter potential, equation (17), in the Earth, which by assumption affects only the flavor eigenstate ν_{s1}, but not ν_{s2}. For simplicity, we take $V^\oplus_{A'}$ to be constant throughout the Earth. We have also introduced the abbreviation

$$\omega \equiv \sqrt{\sin^2 2\theta + (\cos 2\theta - 2EV^\oplus_{A'}/\Delta m^2)^2} \,. \quad (22)$$

Note that equation (21) is valid only in the case where flavor transitions in the Sun are fully adiabatic, which requires [100]

$$\frac{\Delta m^2 \sin^2 2\theta}{2E \cos 2\theta} \gg \left| \frac{\dot{V}^{\odot}_{A'}}{V^{\odot}_{A'}} \right| , \tag{23}$$

where $\dot{V}^{\odot}_{A'}$ denotes the derivative of the non-constant matter potential inside the Sun with respect to distance from the center. In the following, we assume this adiabaticity condition to be fulfilled. Note also that, for sufficiently heavy sterile neutrinos, $V^{\odot}_{A'} \ll |\Delta m^2_{4i}|/2E$, hence the active–sterile mixing angles in matter and vacuum are almost identical: $U^{\odot}_{e4} \sim U_{e4}$, $U^{\odot}_{e5} \sim U_{e5}$.

For oscillation lengths much shorter than the diameter of the Earth, a detector with limited statistics and limited energy resolution will not be able to resolve the individual oscillation peaks, but will only see their average effect. In this case we can make the replacement $\sin^2(\omega \Delta m^2 L^{\oplus}/4E) \to 1/2$ in equation (21). We see that, if the resonance condition

$$2EV^{\oplus}_{A'} \simeq \Delta m^2 \cos 2\theta \tag{24}$$

is fulfilled, the oscillation amplitude inside the Earth can be very large even if the vacuum mixing angle θ is small. If $|U^{\odot}_{e4}|^2 > |U^{\odot}_{e5}|^2$, the probability for detecting a ν_{s1} is larger during the day than it is at night. As discussed above, this diurnal modulation also leads to an annual modulation of the daily average count rate. The length of the day is larger in summer than in winter, therefore, for $|U^{\odot}_{e4}|^2 > |U^{\odot}_{e5}|^2$ ($|U^{\odot}_{e4}|^2 < |U^{\odot}_{e5}|^2$), the average daily count rate is also larger (smaller) in summer than in winter. Note that this type of annual modulation cannot be invoked to explain the modulation signals observed in DAMA [27] and CoGeNT [25] since neither of these experiments has observed the accompanying (and stronger) diurnal modulation [95, 101].

It is also very important to recall that a non-standard matter potential in the Sun ($V^{\odot}_{A'}$) and in the Earth ($V^{\oplus}_{A'}$) for sterile neutrinos is only generated in models in which the Sun and the Earth are not neutral under the gauge group that couples Standard Model particles to the sterile neutrinos. Therefore, the modulation mechanism discussed here will not be effective in models in which the new gauge boson couples to the Standard Model only through kinetic mixing.

It is useful to rewrite the resonance condition (24) as

$$L_{\rm osc} V^{\oplus}_{A'} = 2\pi \cos 2\theta \, , \tag{25}$$

with the oscillation length $L_{\rm osc} = 4\pi E/\Delta m^2$. From this expression we see that for large $V^{\oplus}_{A'}$, i.e. relatively strong coupling between ν_{s1} and ordinary matter the resonance condition can only be fulfilled if the oscillation length is very small, i.e. for very low E or relatively large Δm^2. If $L_{\rm osc} \lesssim 1$ km, matter effects are important even during daytime because detectors are typically located $\gtrsim 1$ km underground. Setting $L_{\rm osc} = 1$ km in equation (25), we find that this happens for

$$\frac{g_e g_\nu}{M^2_{A'}} \gtrsim 0.18 \text{ GeV}^{-2} \, . \tag{26}$$

This should be compared to the corresponding Standard Model quantity $g^2/4M^2_W = 8.2 \times 10^{-6}$ GeV^{-2}.

It is amusing to note that a strong day–night asymmetry combined with the effects of the varying Earth–Sun distance could conspire to give a modulation phase that is very dark matter-like. The amplitude of annual modulation from a day–night asymmetry is at most on the order of 20% for a detector at mid-latitudes, and the peak of such a modulation coincides with the summer solstice around June 21st. The Earth–Sun distance effect is weaker and has a nearly opposite phase, with a minimum on July 4th. The combined effect is a modulation with a maximum total flux occurring on a date earlier than June 21st and closer to early June, which is the canonical peak of the dark matter signal. This scenario may be easily distinguished from a dark matter signal thanks to the strong daily modulation which it predicts (and which has not been seen in DAMA and CoGeNT).

6.4. Zenith angle dependence of Earth matter effects

In the previous section, we have seen that a day–night asymmetry in the sterile neutrino interaction rate in a detector can be generated in models where the oscillation length $L_{\rm osc}$ for oscillations among different sterile neutrino flavors is much smaller than the diameter of the Earth ($\sim 12\,700$ km), but much bigger than the detector's rock overburden (typically of order one kilometer). Phenomenologically very interesting (though extremely fine-tuned) models can be constructed by choosing the mass splitting between the new neutrino mass eigenstates such that $L_{\rm osc}$ is close to either end of this range. This is because the daily averaged distance a solar neutrino must travel inside rock before reaching a detector modulates annually due to the different range of zenith angles under which the detector sees the Sun at different times of the year. Away from the equator, the Sun is higher in the sky at noon in summer as compared to winter. Similarly, in winter the Sun drops lower below the horizon during the night. In figure 6 we show the distribution of neutrino path lengths in matter for solar neutrinos on their way to the Gran Sasso laboratory (where, for instance, the DAMA, CRESST and XENON-100 experiments are located). In the plot we distinguish between the summer months (red histogram) and the winter months (black histogram). We see that both the average path length in matter during daytime and during nighttime varies by an $\mathcal{O}(1)$ factor between summer and winter. Thus, if $L_{\rm osc}$ is around one kilometer or around several thousand kilometers, the oscillation probability can modulate significantly during the year (and also during a day). It is amusing to note that in the case $L_{\rm osc} \sim 1$ km, the precise modulation pattern depends on the latitude of the laboratory, on the detailed topography of the landscape above the detector, and possibly even on the location of the detector within the laboratory. To compute figure 6, we have used topographical data of the Gran Sasso region [102] to determine the rock thickness $d(\Theta, \Phi)$ above the Gran Sasso Laboratory (42° 27' North, 13° 34' East, 963 m above sea level [103]) as a function of the zenith angle Θ and the azimuth angle Φ. For zenith angles below the horizon, we have approximated the Earth as a simple sphere. We have then weighted $d(\Theta, \Phi)$ by the fraction of time the Sun spends at any given point (Θ, Φ) in the sky (or below the horizon) during the time periods indicated in the legend. All computations were done in Mathematica 8.

6.5. Diurnal and annual modulation from neutrino absorption in the Earth

In models that feature sterile neutrinos with sufficiently large couplings to ordinary matter, the sterile neutrinos' scattering cross section can be so large that their mean free path becomes less than the diameter of the Earth. (For constraints on such models and a discussion of the allowed parameter space see section 7 below.) At night, when they have to travel through a substantial amount of matter before reaching a detector, the sterile neutrinos would thus loose all their kinetic energy and become undetectable, whereas during daytime, they could reach the detector unimpeded. This can lead to a very strong daily modulation of the experimental event rate, and due to the different length of day in summer compared to winter, also to annual modulation peaking in summer.

6.6. Modulation from direction-dependent quenching factors

Finally, there is the possibility that temporal modulation of a neutrino scattering signal is induced by direction-dependent solid state effects in a target crystal. This source of modulation is especially interesting for signals which originate from a particular direction such as the Sun, as opposed to signals originating from dark matter which are roughly isotropic, with only a small direction dependence in the velocity spectrum due to the Earth's motion with respect to the dark

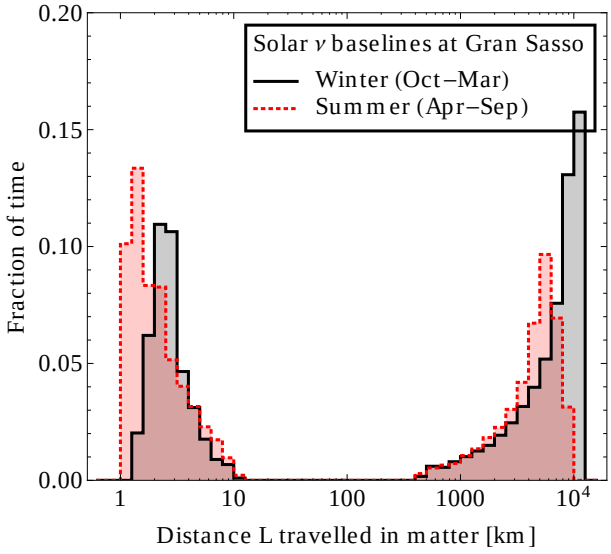

Figure 6: The distribution of the amount of Earth matter a solar neutrino has to travel through in winter (October–March, black histogram) compared to summer (April–September, red histogram) in order to reach a detector in the Gran Sasso Laboratory. To obtain this plot, we have computed the thickness of the rock around the laboratory as a function of the zenith and azimuthal angles (including effects of local topography), and have weighted the result by the fraction of time the detector sees the Sun in any given direction. A very large daily and annual modulation of a sterile neutrino signal may be achieved in models with oscillation lengths around a few kilometers or around several thousand kilometers.

matter halo of the Milky Way. (This directionality in the dark matter velocity distribution as seen from the Earth is usually referred to as the "WIMP wind").

It is well known that the response of a solid state detector to nuclear recoils can be very sensitive to the direction in which the recoil nucleus is traveling with respect to the crystal axes (see for instance [104–109]). In particular, if the initial momentum of the recoiling nucleus is aligned with one of the crystal planes, it is likely to bump into its nearest neighbors, and most of its energy will be converted into phonons. On the other hand, if the recoiling nucleus enters the space between crystal planes and travels along this "channel", it will mostly scatter on electrons, so that a larger fraction of the recoil energy is converted into electronic excitations. In many detectors, only electronic excitations can be detected, so that for these "channeled" events, the ratio between the visible energy and the actually deposited energy (the quenching factor) is larger. The magnitude of blocking and channeling effects is strongly dependent on the target material, the nuclear recoil energy and the temperature at which the detector is operated. In typical dark matter detectors, at most a few per cent of nuclear recoils with a given energy and direction can be channeled, and *typical* channeling fractions are 1–3 order of magnitude smaller [104–108].

Detectors like CDMS or CRESST, which use superconducting phase transition thermometers to measure directly the total deposited energy, are not strongly affected by channeling, and only their background rejection efficiency might change if the fraction of energy going into electronic excitations (scintillation and ionization) varies. On the other hand, experiments like DAMA or CoGeNT, which rely exclusively on electronic signals for their energy measurement, could be strongly affected by direction-dependent quenching factors.

In these experiments, the reconstructed recoil energy spectrum, and thus also the total number of events above threshold, would change as a function of the recoil direction. For conventional

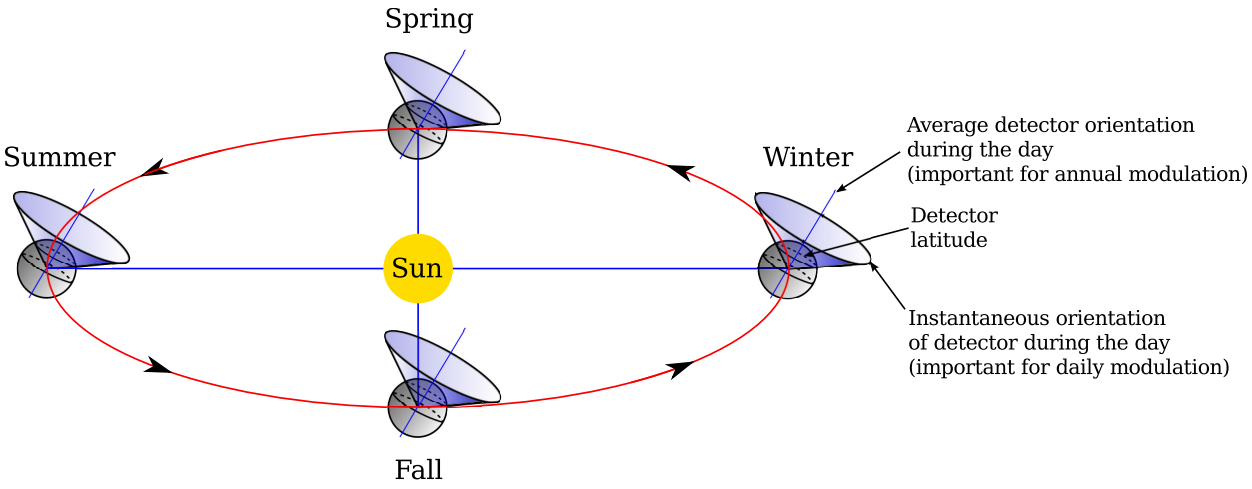

Figure 7: Illustration of the relative orientation of a detector with respect to the solar neutrino flux throughout the year. In blue we show the cones which the detector's normal axis traces out during a day, and in red we show the Earth's trajectory around the Sun. As explained in the text, a detector whose detection efficiency depends on the direction of the incoming particles can observe both diurnal and annual modulation in the solar neutrino signal, and possibly also several higher harmonics of these fundamental frequencies.

signals from the scattering of heavy dark matter particles on nuclei, the rotation of the Earth implies that at different times during the day, the detector sees the "WIMP wind" under different angles, so that one would expect a small modulation in the detection rate during the sidereal day (not the solar day). Direction dependent detection efficiencies would, however, not contribute to annual modulation because the orientation of the Earth's axis relative to the WIMP wind does not change during the year. This can be understood from figure 7, in which the blue cones illustrate the trajectory which the detector's normal axis traces during a day, and the red ellipse depicts the Earth's orbit around the Sun.

The situation is different for signals induced by particles coming from the Sun, such as neutrinos. In this case, direction-dependent detection efficiencies will lead to modulation synchronized with the *solar* day (not the sidereal day) and with the solar year. The exact spectrum of modulation frequencies depends on the specific target material, in particular on the orientation of the preferred directions for channeled nuclear recoils in this material. The important time scales for modulation in this scenario will almost certainly be daily and annually, but semi-annual or other periods are also possible, depending on the symmetries and orientation of the crystal in question.

Modulation signals from direction-dependent quenching factors may be easily identified by rotating the detector and collecting more data.

7. THE PARAMETER SPACE FOR LIGHT GAUGE BOSONS AND NEW CONSTRAINTS

One of the central ingredients of the models discussed in the previous sections is a new, light and feebly coupled $U(1)'$ gauge boson A', the dark photon. The possible existence of such a particle has been considered in the literature in many contexts (unrelated to neutrinos), and strong bounds on the A' mass and couplings have been derived. Therefore, in order to fully assess the viability of our models, we need to make contact with these experimental constraints. In order to keep the discussion brief we will in most cases simply present the existing bounds and refer the reader to the

literature for further details on the physics behind them. We will consider the models discussed in sections 3.2–3.4:

A A $U(1)_{B-L}$ gauge boson with vector couplings to fermions

B A $U(1)'$ gauge boson kinetically mixed with the photon, and with no other couplings to Standard Model particles

C A $U(1)_B$ gauge boson (gauged baryon number)

As we have seen in sections 4 and 5, model A can substantially enhance even the scattering rates of active neutrinos. In model B, on the other hand, the dark photon does not couple to electrically neutral Standard Model particles such as neutrinos, so this model can lead to large neutrino signals in dark matter detectors only if, in addition to the dark photon, there are sterile neutrinos that carry a $U(1)'$ charge. In this case, the dark photon can induce sterile neutrino–electron and sterile neutrino–nucleus scattering, with the latter effect being subdominant. See sections 4 and 5 for details on the phenomenology. Finally, model C can lead to an enhancement of only the neutrino–nucleus scattering rate, while leaving neutrino–electron scattering largely unchanged (except for loop-induced effects), provided that there are "baryonic" sterile neutrinos charged under $U(1)_B$.

In the literature, constraints on light gauge bosons are usually presented in the context of $U(1)'$ bosons coupled only through kinetic mixing (model B), but for many of the relevant processes (see below), a scenario with a $U(1)_{B-L}$ gauge boson is equivalent to such a model. In fact, for any process involving only A' couplings to electrons and protons (but not neutrons or neutrinos), whose electric charges happen to be identical to their $B-L$ charges, a $U(1)_{B-L}$ gauge boson with coupling g_{B-L} and mass $M_{A'}$ is equivalent to a kinetically mixed dark photon, equation (12), with kinetic mixing parameter $\epsilon = g_{B-L}/e \times [1 + g_{B-L}^2/e^2]^{-1/2}$ and mass $M_{A'}^2 \times (1 + g_{B-L}^2/e^2)^{-1}$. At the formal level, this equivalence can be demonstrated by transforming the $B-L$ model according to $A \to A - g_{B-L}/e \times A'$, and then rescaling the A' field. (Here, A is the Standard Model photon.) For $U(1)_B$ gauge bosons, model C, many of the existing constraints do not apply at all (see below).

Where applicable, we will also comment on variations of models A–C, in particular scenarios with sterile neutrinos ν_s charged under $U(1)'$, where $A' \to \bar{\nu}_s \nu_s$ decays can modify the phenomenology. We will also mention "chameleon" models, i.e. models in which the A' mass changes as a function of the background matter density [20, 67, 76], which can also change or eliminate bounds.

The various constraints on $U(1)_{B-L}$ gauge bosons are shown in the top panel of figure 8, and the constraints on light gauge bosons kinetically mixed with the photon are shown in the bottom panel. Constraints on all three models considered here are also summarized in table I. To obtain the top panel of figure 8, we have translated the limits on kinetic mixing from [65, 66] into limits on a $B-L$ gauge coupling g_{B-L} by replacing ϵ with g_{B-L}/e, where e is the unit charge. (In the case of the constraint from Υ decays, the transformation is $\epsilon \to g_{B-L}/2e$ because the electric charge of the bottom quark is twice its $B-L$ charge.) It is important to note that there are additional constraints in the $U(1)_{B-L}$ case (model A) compared to model B (kinetic mixing), namely from Borexino and from long-range force searches [60–63] (see below for details). The latter apply also to the $U(1)_B$ model (model C).

The bounds in the plot are color coded: Regions colored in dark blue represent the most robust limits from laboratory experiments. In particular, these limits are still valid if the new light gauge boson is subject to strong chameleon effects. Limits in lighter shades of blue are sensitive and may be evaded with chameleon effects (the lightest shades of blue are reserved for limits that have not been worked out in detail and are less robust. Limits shown in red apply to the $U(1)_{B-L}$ model (A), but not models in which the A' couples to Standard Model particles only via kinetic mixing (model B). Green limits apply only if there are, in addition to the A' gauge boson, sterile neutrinos charged under $U(1)'$ with the coupling constant and mixing angle indicated in the plot.

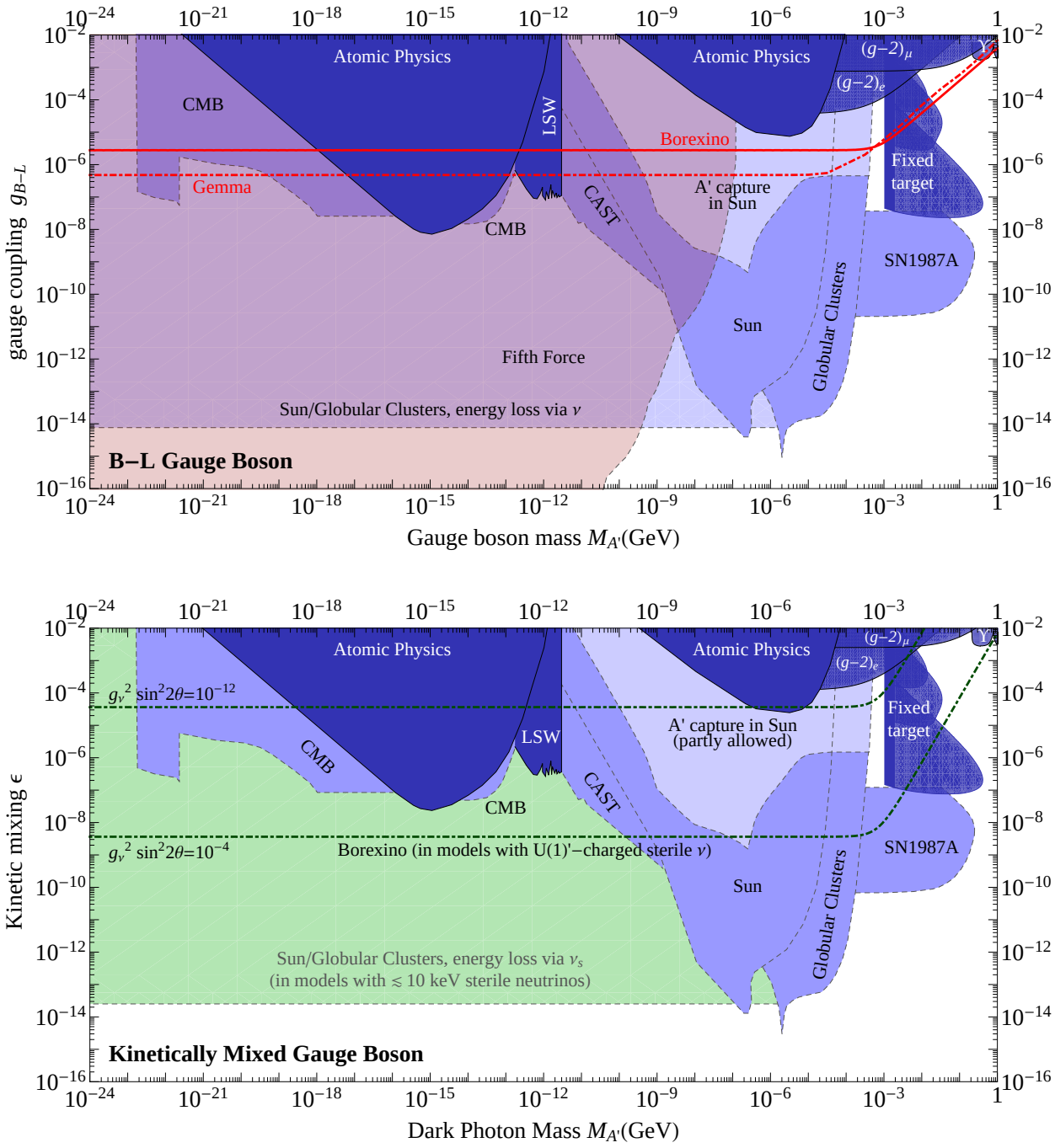

Figure 8: *Top:* Constraints on a $U(1)_{B-L}$ gauge boson (model A, section 3.2) with coupling g_{B-L} and mass $M_{A'}$. *Bottom:* Constraints on light A' gauge bosons kinetically mixed with the photon (model B, section 3.3) as a function of the A' mass and the kinetic mixing parameter ϵ. The various bounds are briefly explained in the text. Limits shown in dark blue are the ones that *cannot* be evaded even if the mass of the A' depends strongly on the local matter density (so-called chameleon effects [20, 67, 76]). The red exclusion regions apply only to the $U(1)_{B-L}$ models (A), but not models with only kinetic mixing (model B). The green exclusion regions apply only if the model contains sterile neutrinos directly charged under $U(1)'$. Most limits are taken from the compilation in [65], see text for further references. To our knowledge, the Borexino and GEMMA limits shown here have not been discussed before.

The individual constraints, which are also summarized in table I, are:

1. **Anomalous magnetic moment of the electron and the muon ("$(g-2)_e$", "$(g-2)_\mu$").** A new gauge boson coupling to leptons (Models A and B, but not C) will contribute to the magnetic moment of the electron and the muon at the one loop level, see for example [110]. Note that a model with parameters just below the $(g-2)_\mu$ exclusion line in figure 8 could explain the currently observed deviation of $(g-2)_\mu$ from its Standard Model prediction [111].

2. **Fixed target experiments.** Electron and proton beam dump experiments have placed limits on dark photons produced in the target and decaying to electron–positron pairs, see [112–114]. Obviously, this technique can only constrain dark photons with $M_{A'} > 2m_e$. The fixed target constraints shown in figure 8 apply directly only to models A and B. In C, A' decays to electron–positron pairs would be loop-suppressed, so the bounds would become much weaker in this case. Even in model B, the constraints are not robust if the model contains sterile neutrinos directly charged under $U(1)'$ (the case of most interest to us in this work), since in this case, the branching ratio for A' decay into e^+e^- pairs is greatly reduced. It is expected that fixed target constraints will be significantly improved by the APEX experiment (see [115] for first results from this experiment).

3. **Υ decays.** Decays of Υ mesons to a photon plus a dark photon, with the latter decaying further to $\mu^+\mu^-$, are constrained by B-factory experiments [116]. Note that for a $U(1)_{B-L}$ boson these constraints are modified by an $\mathcal{O}(1)$ factor compared to the case of a kinetically mixed dark photon because the electric charge of the bottom quark is different from its $B-L$ charge. In model B, the constraint is avoided if a fast A' decay mode to sterile neutrinos exists. The $U(1)_B$ model is not directly constrained by $\Upsilon \to \gamma\mu^+\mu^-$, but searches for hadronic decays could be used to set limits, which would be strongest for $M_{A'}$ around the Υ mass ~ 10 GeV [117, 118].

4. **Atomic physics constraints.** By comparing the energy differences between excited atomic states to the energy differences measured between lower-lying atomic transitions, anomalous corrections to the Coulomb force at atomic distance scales can be constrained [119]. These constraints apply only to models in which the dark photon couples to electrons, i.e. models A and B, but not C.

5. **Supernova 1987A ("SN1987A").** A dark photon may be produced in the core of a supernova and contribute to its energy loss. By requiring that in Supernova 1987 A, the energy loss in dark photons was not larger than the known energy loss in neutrinos (10^{53} erg/s), constraints on the A' mass and coupling can be derived [66]. Note that these bounds cover only a limited range of A' couplings: for too small couplings, the energy loss in dark photons is small; for too large couplings, the supernova is opaque even to dark photons, so that anomalous energy losses occur only in a thin outer shell. Note also that A' emission in a supernova is mostly due to A' radiation off protons and neutrons. Therefore, the constraints apply to all three models considered here. Let us also remark that supernova constraints can be avoided altogether in models where the dark photon feels strong chameleon effects, so that its effective mass inside the supernova is higher than its mass in vacuum [20].

6. **Solar constraints ("Sun").** A dark photon can also be produced by thermal radiation in the Sun. Unlike for supernovae, A' radiation in stars is dominated by emission off electrons or, more precisely, by the conversion of plasma excitations (so-called plasmons) into dark photons. Requiring that the solar luminosity in dark photons is smaller than the known luminosity in photons places a strong bound on A' bosons in a wide mass window around

the solar plasmon resonance at $M_{A'} \sim 100$ eV [64]. As for the supernova case, this bound is not robust at large ϵ, where dark photon absorption inside the Sun becomes relevant. To our knowledge, dark photon dynamics in this regime has not been considered in the literature, but since it is clear that dark photon absorption will reduce the problematic anomalous solar energy loss due to A' emission, part of the region labeled "A' capture in Sun" in figure 8 may still be allowed [64]. Indeed, the results from [120] (derived for keV-scale *scalars*) suggest that $\mathcal{O}(\text{few} \times 10 \text{ keV})$ particles may still be acceptable, while lower masses can be ruled out by requiring anomalous heat transfer mechanisms inside the Sun to be small. We expect solar constraints to be most relevant to models A and B, in which the dark photon couples to electrons. In model C, the only available A' production mechanism is radiation off nuclei, which we expect to be much smaller than radiation off electrons. However, to our knowledge, this has never been worked out in detail.

If the A' boson couples to neutrinos, the solar constraint also depends on neutrino dynamics. In the $U(1)_{B-L}$ model (model A), where the A' boson couples directly to the active neutrinos, low-energy neutrinos produced in plasmon decay can carry away energy even if the dark photon cannot because its mass is outside the plasmon resonance region. In the literature, the corresponding constraints are usually referred to as "minicharged particle limits" [65, 72] and in figure 8, they are approximately indicated by the region labeled "Sun/Old Stars, energy loss via ν". At very large g_{B-L}, energy loss through low-energy neutrinos is not effective because these neutrinos cannot leave the Sun due to their large scattering cross sections. However, since neutrino scattering is suppressed by g_{B-L}^4, we estimate that the large g_{B-L} values required for this to happen are already disfavored by other constraints, for instance atomic physics constraints and $g-2$ limits. Moreover, in scenarios with very large g_{B-L}, also the spectrum of higher energy solar neutrino from nuclear fusion may be distorted, in potential conflict with experiments. While a detailed study of these issues is beyond the scope of this work, we estimate that in the $U(1)_{B-L}$ model, the region labeled "A' capture in Sun" in figure 8 is ruled out by minicharged particle limits. In the $U(1)'$ model with kinetic mixing (model B), on the other hand, minicharged particle constraints are relaxed since the A' in this case does not couple to active neutrinos, but only to hypothetical sterile neutrinos. If the latter are heavier than ~ 10 keV, many minicharged particle limits no longer apply [72]. (For $\epsilon \gtrsim 10^{-9}$, even larger masses, $\gtrsim$ few hundred keV–several MeV may be required to avoid the constraints from [72].) Even if the sterile neutrinos are lighter, they may avoid solar constraints more easily if ϵ is large. The reason is that for a $U(1)'$ gauge coupling of order one, the scattering of sterile neutrinos is suppressed only by ϵ^2 (just like A' absorption, and compared to g_{B-L}^4 in the $U(1)_{B-L}$ model), i.e. sterile neutrinos in this model can be more easily absorbed in the Sun. For instance, for $M_{A'} = 1$ keV, $\epsilon = 10^{-5}$, the sterile neutrino mean free path is less than 10 cm. The average energy loss per scattering is of order 10 eV, i.e. a 1 MeV neutrino will have lost all of its kinetic energy after traveling for ~ 10 km. We therefore estimate that the $U(1)'$ model with kinetic mixing, and with $M_{A'} \sim 1$ keV, $\epsilon \gtrsim 10^{-8}$, is not robustly excluded, even if it contains sterile neutrinos acting as minicharged particles. An in-depth study of the dark photon and sterile neutrino dynamics in the large ϵ regime is a possible direction for future work.

As a final remark, we note that chameleon effects could also help circumvent the solar energy loss bound if the A' effective mass is higher in the solar core than in vacuum [20, 76].

7. **Cooling of stars in globular clusters.** Evolved stars, on the horizontal branch in the Hertzsprung-Russell (temperature vs. luminosity) diagram, can be used to set limits on energy loss due to dark photons in the same way in which solar constraints are derived. A particularly promising target for the study of these stars are globular clusters since the initial

conditions for star formation in these objects are the same throughout the cluster. Since horizontal branch stars have a higher temperature than the Sun the corresponding limits reach out to higher A' masses. Like the constraints from solar cooling, they also disappear at large A' coupling $\gtrsim 10^{-6}$, as approximately indicated in figure 8. They also disappear in chameleon models, whereas their applicability to models without A' couplings to electrons (model C) has not been studied in detail yet.

8. **The CAST experiment.** Helioscopes such as the CERN Axion Solar Telescope (CAST) [121], which are looking for electromagnetic signals in a dark, shielded cavity are sensitive to dark photons from the Sun entering the cavity and oscillating back into visible photons inside. This process can be used to set strong limits on the dark photon coupling in a mass region where the expected dark photon flux from the Sun would be large [64]. Helioscope bounds suffer from similar model-dependencies as solar and stellar constraints; in addition, they can be avoided if the dark photon can decays, for instance to neutrinos, before reaching the Earth.

9. **Light shining through walls ("LSW").** In this type of experiments, one directs an intense laser beam onto an opaque wall and searches for residual signals behind the wall. Conversion of laser photons into dark photons and back into visible photons could lead to such signals, and thus these experiments can be used to set limits on the dark photon mass and couplings [122]. These limits do not apply to $U(1)_B$ bosons (model C).

10. **CMB constraints.** A dark photon would mix with the visible photon in a frequency dependent way, and this effect can attenuate the black body spectrum of the CMB [123] which was measured precisely by the FIRAS instrument on board the COBE satellite [124]. These bounds may be avoided if the mass of the dark photon is higher in the dense early Universe due to chameleon effects.

11. **Borexino.** Due to its large fiducial volume and the large solar neutrino flux, Borexino is quite sensitive to modifications of the neutrino–electron scattering rate. The non-observation of any anomalous signals can be translated into constraints on the couplings of dark photons to neutrinos and electrons. In particular, we require that the neutrino–electron scattering rate in Borexino should not be more than 8% [34] above the Standard Model prediction [43]. The solid red line in the top panel of figure 8 shows the Borexino constraint for the case of a $U(1)_{B-L}$ model (mode A), whereas the green lines in the bottom panel of figure 8 are for models of type B (a kinetically mixed $U(1)'$ gauge boson), but including also sterile neutrinos charged under $U(1)'$.

12. **GEMMA.** The GEMMA spectrometer at the Kalinin Nuclear Power Plant [42] searches for anomalous contributions to neutrino–electron scattering, with the aim of constraining neutrino magnetic moments. To derive limits on the couplings of a dark photon to electrons, we use the data shown in figure 8 of reference [125][11] and compare it to the A' model using a simple χ^2 test. We require the difference in χ^2 between the A' model and the Standard Model to be < 3.84, corresponding to a one-sided 90% C.L. upper limit.

    Since GEMMA is looking for neutrino–electron scattering, it is insensitive to the $U(1)_B$ model (model C), and also to the $U(1)'$ model with kinetic mixing (model B), unless there

[11] Note that the strong limit on the neutrino magnetic moment derived in [125] was based on a theoretical calculation [126] that was later revised [127, 128]. We therefore do not consider this limit here, but we can still use the data presented in [125] to derive our own limits on the parameter space of dark photons.

are sterile neutrinos charged under $U(1)'$ and heavy enough to be produced in oscillations of active neutrinos over distance scales of order 10 m (see section 4.1).

13. **Fifth force searches.** On distance scales $\gtrsim 10$ nm ($M_{A'} \lesssim 100$ eV), new long range forces are tightly constrained by precision tests of the gravitational, Casimir, and van der Waals forces. Since these experiments probe interactions between electrically neutral bodies, they are sensitive to $U(1)_{B-L}$ or $U(1)_B$ gauge bosons (models A and C), but not to gauge bosons coupled only through kinetic mixing (model B).

    Results from fifth force searches are often reported as limits on an anomalous Yukawa-type contribution to the gravitational potential (see for instance section 24 in [61] or figure 28 in [60]) of the form $V_{\rm new} = -G_N m_1 m_2/r \times \alpha_G \exp(-M_{A'} r)$. Here, G_N is the gravitational constant, m_1, m_2 are the masses of the test bodies, r is the distance between their centers of mass, α_G is a coupling constant, and $M_{A'}$ is the mass of the new force mediator, or equivalently the inverse range of the new force. Constraints on α_G can be translated into constraints on a $B-L$ gauge coupling constant g_{B-L} according to $g_{B-L}^2 = \alpha_G G_N (m_1/q_{B-L,1})(m_2/q_{B-L,2})$, with $q_{B-L,1}$ and $q_{B-L,2}$ being the $B-L$ charges of the test bodies. In practice, $m_j/q_{B-L,j} \simeq 0.5$ GeV is just the nucleon mass multiplied by the inverse neutron fraction of the target material. (For the case of a $U(1)_B$ force, q_{B-L} should be replaced by q_B, and $m_j/q_{B,j} \simeq 1$ GeV.)

    Among the most sensitive tests of the inverse square law of gravitational interactions over laboratory distance scales are the experiments carried out by the Eöt-Wash group [62, 63]. These experiments restrict the coupling strength of a $U(1)_{B-L}$ boson to be smaller or similar to the strength of gravitational interactions for $M_{A'} \lesssim 0.01$ eV (see for instance figure 1 of reference [62]; for the $U(1)_B$ case, the replacement $g_{B-L} \to g_B \sqrt{2} N/(Z+N) \simeq 0.8 g_B$ should be made in this figure). Such a gauge boson could thus never lead to an observable signal in a dark matter detector.

    At somewhat larger masses or smaller distance scales, the strongest constraints come from tests of the Casimir force, i.e. the small attractive force that the zero point energy of the electromagnetic quantum field induces between conducting objects that are brought very close to each other (distance 10^{-8}–10^{-3} m) [60, 61]. At these distances, the boundary conditions imposed on the electromagnetic field by the conducting test bodies lead to a measurable modification of the electromagnetic vacuum energy. At even short distances, down to 10^{-9} m, also tests of van der Waals forces become important [60, 61]. Constraints on g_{B-L} from tests of the Casimir effect are weaker than Eöt-Wash limits for $M_{A'} \lesssim 0.01$ eV, but they extend to larger gauge boson masses and still provide a limit $g_{B-L} \lesssim 10^{-6}$ at $M_{A'} = 100$ eV.

We should mention that the small allowed region between the globular cluster and fixed target constraints can be partially ruled out in models with *only* a dark photon (but no sterile neutrinos) using the requirement that the intergalactic diffuse photon background is not modified by $A' \to 3\gamma$ decays, that the black body spectrum of the CMB is not modified, and that the effective number of light degrees of freedom at the epoch of Big Bang nucleosynthesis agrees with observations [129]. The constraints can be avoided if the dark photon decays dominantly into neutrinos (active neutrinos in the $U(1)_{B-L}$ model and sterile neutrinos in the $U(1)'$ model with kinetic mixing).

Moreover, for dark photons with $\mathcal{O}$(keV) masses or above, the dark photons themselves can act as "lukewarm dark matter" [129], potentially overclosing the Universe. Constraints of this type can be avoided by the same mechanisms as for heavy sterile neutrinos (see discussion at the end of section 3.3).

	$U(1)_{B-L}$ (vector couplings) (Model A)	Kinetically mixed (Model B)	$U(1)_B$ (vector couplings) (Model C)
$g-2$	✓	✓	✗
Fixed Target	✓	✓	✗[a]
Υ	✓	✓	✗[b]
Atomic physics	✓	✓	✗
Sun/Clusters/CAST	✓	✓	?
SN1987A	✓	✓	✓
LSW	✓	✓	✗
CMB	✓	✓	?
Borexino	✓	only if ν_s exist	✗
GEMMA	✓	✗	✗
Fifth force	✓	✗	✓

[a]By looking for hadronic A' decays, fixed target experiments could set limits even on a $U(1)_B$ gauge boson (model C). To our knowledge, no such analysis has, however, been done.

[b]Studies of hadronic Υ decays could be used to set limits, which would be strongest for $M_{A'}$ similar to the Υ mass, around 10 GeV [117, 118].

Table I: Applicability of the various constraints on new light gauge bosons to the three models considered here. '✓' indicates constraints that apply to a given model (the exact strengths of these constraints may still differ by an $\mathcal{O}(1)$ factor between models), '✗' indicates constraints that are not applicable, and '?' stands for constraints for which a dedicated study would be required to determine their applicability.

It is worthwhile to recapitulate which regions of parameter space are most relevant to the phenomenology of neutrino signals in dark matter detectors. For the kinetic mixing model (model B), dark photon masses in a window from ~ 10 keV to ~ 1 MeV, are of most interest. Masses below 1 eV can also be considered, provided that sterile neutrinos are sufficiently heavy ($\gtrsim 10$ keV–several hundred keV) to avoid bounds on minicharged particles. The kinetic mixing parameter ϵ required to produce sizeable signals depends on the sterile neutrino flux and could vary between 10^{-12} and 10^{-5}. For the $U(1)_{B-L}$ model (model A, there may be a small region of interest around $M_{A'} \sim 50$ keV, $g_{B-L} \sim 10^{-6}$. For other masses or couplings, chameleon effects can be introduced to evade astrophysical and fifth force limits. The $U(1)_B$ model (model C) is far less constrained than the other two and can yield interesting phenomenology in the whole mass range considered (1 GeV and below).

8. CONCLUSIONS

In this paper, we have discussed the rich phenomenology of standard and non-standard solar neutrino signals in dark matter direct detection experiments. In particular, we have considered models featuring a neutrino magnetic moment, as well as scenarios with a "dark photon" A' (a light, weakly coupled new gauge boson). We have shown that in these scenarios neutrino–electron and neutrino–nucleus scattering can be much stronger than Standard Model weak interactions at the low recoil energies to which dark matter detectors are sensitive, while being consistent with constraints from higher energy experiments such as Borexino and SNO. If we moreover assume that a small fraction of solar neutrinos has oscillated into new "sterile" flavors, whose couplings to the dark photon are much less constrained than those of Standard Model particles, the scattering rates can be large enough to explain at least some of the recently reported anomalous signals from dark matter experiments.

We have also discussed possible sources of temporal variations in the neutrino count rate, in particular the annual variation of the Earth–Sun distance (possibly in conjunction with oscillation effects, if the active–sterile oscillation length is not too much smaller than one astronomical unit), neutrino absorption in the Earth, diurnal and annual modulation due to Earth matter effects, and temporal modulation effects in detectors whose efficiency depends on the direction of the incoming particles, for instance because of ion "channeling" effects.

We conclude that dark matter detectors, with their low energy thresholds, can be very sensitive to new physics in the neutrino sector, in particular if the new effects are strongest at low energy and are thus hidden from dedicated neutrino experiments, whose recoil energy thresholds are at least a few hundred keV. Signals from neutrino–electron scattering and neutrino–nucleus scattering can be easily confused with dark matter scattering, especially when the signal consists of only a few events so that detailed investigations of the event spectrum or of temporal modulation effects are not possible. This is an important consideration for the present generation of detectors, but even more so for future experiments, whose large mass and reduced background will make them more sensitive to both dark matter and neutrino signals. On the other hand, our study also shows that dark matter detectors are powerful tools to constrain or discover neutrino physics beyond the Standard Model.

Note added: Shortly after the present paper was completed, an interesting related work by Pospelov and Pradler appeared on the arXiv [130].

Acknowledgments

The authors would like to thank Rouven Essig, Francesc Ferrer, Kai Schmidt-Hoberg, Maxim Pospelov, Surjeet Rajendran, Carlos Savoy, Ian Shoemaker, Neil Weiner, our anonymous referee, and especially Toshihiko Ota and Javier Redondo for interesting and useful discussions. JK is grateful to the Aspen Center for Physics (supported by the National Science Foundation under Grant No. 1066293), where part of this work has been carried out. PANM would like to thank Fermilab for kind hospitality and support during his visits. PANM is supported by the Fundação de Amparo à Pesquisa do Estado de São Paulo and by the European Commission under contract PITN-GA-2009-237920. Fermilab is operated by Fermi Research Alliance, LLC, under contract DE-AC02-07CH11359 with the United States Department of Energy.

Appendix A: MODELS WITH HEAVY STERILE NEUTRINOS

In section 4 we have considered heavy sterile neutrino with masses of order several hundred keV, which led to interesting features in the recoil energy spectrum (see figure 3) and helped us avoid constraints on neutrino–electron scattering from XENON-100. On the other hand, in order to get a large enough scattering rate at low energies, the dark photon which mediates the interactions between sterile neutrinos and electrons has to be fairly light, at or below ~ 10 keV. Furthermore the heavy sterile neutrino needs to mix with the light active neutrinos to be produced in the Sun. The product of couplings and mixing angles $g_e g_\nu \sin\theta$ should be of order 10^{-11}, i.e. with $g_\nu \lesssim 1$ from perturbativity and $g_e \lesssim 10^{-5}$ (see figure 8), this translates into the requirement $\sin\theta \gtrsim 10^{-6}$

Achieving this within a see-saw model similar to the one introduced in section 3 (equations (12) and (13)) is not possible because in such models the mass of the sterile neutrino is of order $\langle H' \rangle^2 / M_R \ll \langle H' \rangle$, $M_{A'}$ when the right-handed neutrinos are very heavy.

Apart from the neutrino masses, we also need to generate an appropriate mixing matrix. In particular, in order for the sharp drop in the spectra visible in figure 3 to occur, the electron recoil signal has to be dominated by scattering of the heavy mass eigenstate ν_4 rather than by scattering

of the light mass eigenstates ν_1, ν_2, ν_3 through their small ν_s admixture. (Remember that it is the the sterile *flavor* eigenstate ν_s which is charged under the new gauge group.) This requires the leptonic mixing matrix element U_{e4} (which gives the ν_4 admixture to the electron neutrino) to be much larger than the elements U_{s1}, U_{s2}, U_{s3} (which give the ν_s component of the light mass eigenstates).

Building a model that satisfies all these requirements requires some engineering, but is certainly not impossible, as we now show. We add a pair of sterile neutrinos, one of them (say, ν_{sL}) charged under $U(1)'$ and the other one (ν^c_{sR}) neutral (anomalies can be taken care of by introducing extra spectator fermions). The Dirac mass of the sterile neutrinos is thus proportional to $\langle H' \rangle$, which we will take to be around 800 keV. The mass of the dark photon is also proportional to $\langle H' \rangle$, but may be smaller if the $U(1)'$ gauge coupling is smaller than one. For instance, let us assume a gauge coupling of order 0.01 to give the dark photon a mass around 10 keV. The presence of the H' vev also allows us to write mixing terms between active and sterile neutrinos, particularly between the left handed sterile and the right handed active states. The full neutrino mass matrix is

$$-\mathcal{L}_m \supset \overline{\psi^c_\nu} \left(\begin{array}{cc|cc} 0 & Y^*_\nu \langle H \rangle & 0 & Y^*_{\nu 4} \langle H \rangle \\ Y^T_\nu \langle H \rangle & M_R & Y'^*_s \langle H' \rangle & M_{R,14} \\ \hline 0 & Y'^T_s \langle H' \rangle & 0 & Y^*_s \langle H' \rangle \\ Y^T_{\nu 4} \langle H \rangle & M^T_{R,14} & Y^T_s \langle H' \rangle & M_{R,44} \end{array} \right) \psi_\nu \,. \tag{A1}$$

where we have placed all neutrinos in a vector $\psi_\nu = [\nu_L, (\nu_R)^c, \nu_{sL}, (\nu_{sR})^c]$, and flavor indices are suppressed. If there are, in addition to the three active neutrino flavors and their right-handed partners, n_s left-handed sterile neutrinos and the same number of right-handed sterile neutrinos, Y_ν and M_R are understood to be 3×3 matrices, $Y_{\nu 4}$, Y_s, and $M_{R,14}$ are $3 \times n_s$ matrices, and Y_s, $M_{R,44}$ are $n_s \times n_s$ matrices.

To obtain a model with the desired masses and mixing angles, we will assume that $Y_{\nu 4}$, $M_{R,14}$, and $M_{R,44}$ are negligibly small. This could, for instance, be justified by declaring sterile lepton number (carried by ν_{sL} and ν_{sR}) a global symmetry only broken by the spurion Y'_s. Another possibility is to introduce *two* $U(1)'$-breaking Higgs fields, H'_1 and H'_2, with only H'_1 carrying sterile lepton number. Then, the term $Y'^*_s \langle H' \rangle$ in equation (A1) would be replaced by $Y'^*_s \langle H'_1 \rangle$, and the term $Y^*_s \langle H' \rangle$ would be replaced by $Y^*_s \langle H'_2 \rangle$. The terms $M_{R,14}$, $M_{R,44}$, and $Y^*_{\nu 4} \langle H \rangle$, on the other hand, would be absent.

If we set $Y_{\nu 4}$, $M_{R,14}$, and $M_{R,44}$ to zero and assume $M_R \gg \langle H \rangle, \langle H' \rangle$ in equation (A1), we find that to leading order in the small masses, the admixture of the $\mathcal{O}(\langle H' \rangle)$ mass eigenstates to the left-handed active flavor eigenstates is

$$|U_{e4}| \sim \frac{Y_\nu Y'_s}{\sqrt{2} Y_s} \frac{\langle H \rangle}{M_R} \,. \tag{A2}$$

The admixture of the $U(1)'$-charged flavor eigenstate ν_{sL} to the light $\mathcal{O}(\langle H \rangle^2 / M_R)$ mass eigenstates, on the other hand, vanishes to leading order as desired.

As is clear from equation (A2), a standard seesaw mechanism with $M_R \sim 10^{15}$ GeV will produce mixing angels which are too small. However an electroweak-scale seesaw with $M_R \sim 100$ GeV can easily yield mixings that are large enough. For example, taking Y_s and Y'_s of order one, and requiring the active neutrino masses $m_\nu \sim (Y_\nu \langle H \rangle) M_R^{-1} (Y_\nu \langle H \rangle)$ to be at the 0.1 eV scale, gives a mixing angle of

$$|U_{e4}| \sim 10^{-6} \left(\frac{100 \text{ GeV}}{M_R} \right) . \tag{A3}$$

In order to produce spectra that are close to those observed by DAMA and CoGeNT one can pick $g_\nu \sim 1$ and $g_e \sim 10^{-5}$, which is not ruled out by the constraints from section 7.

Appendix B: EARTH MATTER EFFECTS ON SOLAR NEUTRINOS

In this appendix we explain in detail how Earth matter effects in the sterile neutrino sector can lead to daily modulation (see section 6.3) [99]. We assume a model with two sterile flavor eigenstates ν_{s1} and ν_{s2}, with ν_{s1} giving the strongest signal in the detector. Thus, we are interested in the probability for $\nu_e \to \nu_{s1}$ transitions. As in section 6.3, we make the simplifying assumption that the new, mostly sterile, mass eigenstates ν_4 and ν_5 are so heavy that they cannot be produced in a coherent superposition with the light mass eigenstates ν_1, ν_2, ν_3. We do assume, however, that coherence between ν_4 and ν_5 is possible due to a small mass splitting. As the neutrinos are produced in the core of the Sun, and as we assume the oscillation length to be much smaller than the size of the Sun's core, the solar neutrino flux at the Earth can be treated as an *incoherent* mixture of ν_4 and ν_5. Hence, the computation of the probability $\nu_e \to \nu_{s1}$ is two-step: first, we need to determine the amount of $\nu_{4,5}$ that exit the Sun; then we need to calculate the probability of detecting these mass eigenstates as ν_{s1} after they have traveled a distance $L^\oplus$ in the Earth. Finally, we perform an incoherent sum, that is we compute

$$P(\nu_e \to \nu_{s1}) = P_\odot(\nu_e \to \nu_4) P_\oplus(\nu_4 \to \nu_{s1}) + P_\odot(\nu_e \to \nu_5) P_\oplus(\nu_5 \to \nu_{s1}), \tag{B1}$$

where $P_\odot$ and $P_\oplus$ are the transition probabilities in the Sun and in the Earth, respectively.

Since only the two flavors ν_{s1} and ν_{s2} are relevant to us, we can define an effective two-flavor rotation matrix with mixing angle θ

$$U^\theta = \begin{pmatrix} \cos\theta & \sin\theta \\ -\sin\theta & \cos\theta \end{pmatrix}. \tag{B2}$$

We denote the vectors of the vacuum mass basis, flavor basis and the effective mass basis in Earth matter by $|\nu_i\rangle$, $|\nu_\alpha\rangle$, and $|\nu_i^\oplus\rangle$, respectively. The relations between them are given by

$$|\nu_\alpha\rangle = U^{\theta *}_{\alpha i} |\nu_i\rangle \qquad \text{and} \qquad |\nu_\alpha\rangle = U^{\oplus *}_{\alpha i} |\nu_i^\oplus\rangle\,, \tag{B3}$$

where $U^\oplus$ is the effective mixing matrix in Earth matter, which has the same form as equation (B2), but with θ replaced by the effective mixing angle in Earth matter, $\theta_\oplus$, which is obtained when the full Hamiltonian is diagonalized. Concretely, working in the flavor basis we have

$$H = \frac{1}{4E} U^\theta \begin{pmatrix} -\Delta m^2 & 0 \\ 0 & \Delta m^2 \end{pmatrix} U^{\theta\dagger} + \begin{pmatrix} V^\oplus_{A'} & 0 \\ 0 & 0 \end{pmatrix}, \tag{B4}$$

(with $\Delta m^2 \equiv m_5^2 - m_4^2$) and

$$U^{\oplus\dagger}\, H\, U^\oplus \equiv \mathrm{diag}(-\Delta m^2_\oplus/4E\ ,\ \Delta m^2_\oplus/4E)\,. \tag{B5}$$

It is easy to show that

$$\cos 2\theta^\oplus = \frac{\Delta m^2 \cos 2\theta - 2EV^\oplus_{A'}}{\Delta m^2_\oplus} \qquad \text{and} \qquad \sin 2\theta^\oplus = \frac{\Delta m^2 \sin 2\theta}{\Delta m^2_\oplus}\,, \tag{B6}$$

where

$$\Delta m^2_\oplus = \omega\, \Delta m^2 = \Delta m^2 \sqrt{\sin^2 2\theta + (\cos^2 2\theta - 2EV^\oplus_{A'}/\Delta m^2)^2}\,. \tag{B7}$$

Now, we calculate $P_\oplus(\nu_4 \to \nu_{s1}) = |\langle\nu_{s1}|e^{-iHL_\oplus}|\nu_4\rangle|^2$. With the abbreviations $c_\theta \equiv \cos\theta$, $s_\theta \equiv \sin\theta$, $c_\oplus \equiv \cos\theta_\oplus$ and $s_\oplus \equiv \sin\theta_\oplus$, we find

$$\left|\langle\nu_{s1}|e^{-iHL_\oplus}|\nu_4\rangle\right|^2 = \left|\begin{pmatrix}1 & 0\end{pmatrix}\begin{pmatrix}c_\oplus & s_\oplus\\ -s_\oplus & c_\oplus\end{pmatrix}\begin{pmatrix}e^{+i\Delta m^2_\oplus L_\oplus/4E} & 0\\ 0 & e^{-i\Delta m^2_\oplus L_\oplus/4E}\end{pmatrix}\begin{pmatrix}c_\oplus & -s_\oplus\\ s_\oplus & c_\oplus\end{pmatrix}\begin{pmatrix}c_\theta\\ -s_\theta\end{pmatrix}\right|^2 \tag{B8}$$

$$= \cos^2\theta - \sin^2 2\theta \frac{2EV^\oplus_{A'}}{\omega^2\Delta m^2}\sin^2\left(\frac{\omega\Delta m^2 L_\oplus}{4E}\right) \tag{B9}$$

In the first line we have used the relations (B3), and the third line then follows from simple algebraic manipulations. It is straightforward to see that to obtain $P_\oplus(\nu_5 \to \nu_{s1})$ we just need to replace $\cos^2\theta$ by $\sin^2\theta$ and reverse the sign of the second term.

To complete the calculation of $P(\nu_e \to \nu_{s1})$, we need $P_\odot(\nu_e \to \nu_{4,5})$. The probability for producing the matter eigenstates corresponding to $\nu_{4,5}$ at the center of the Sun is given by $|U^\odot_{e4,5}|^2$, and since the adiabaticity condition (23) is well fulfilled (unless $\sin 2\theta$ is tiny, in which case we would not expect an observable signal from sterile neutrino scattering anyway), this is also the probability that a solar neutrino exits the Sun as $\nu_{4,5}$, i.e.

$$P_\odot(\nu_e \to \nu_{4,5}) = |U^\odot_{e4,5}|^2 . \tag{B10}$$

Plugging (B10) and (B9) into (B1), we obtain equation (21).

[1] A. Gutlein et al. (2010), 1003.5530.
[2] A. Aguilar et al. (LSND), Phys. Rev. **D64**, 112007 (2001), hep-ex/0104049.
[3] A. Aguilar-Arevalo et al. (The MiniBooNE Collaboration), Phys.Rev.Lett. **105**, 181801 (2010), 1007.1150.
[4] T. Mueller, D. Lhuillier, M. Fallot, A. Letourneau, S. Cormon, et al. (2011), 1101.2663.
[5] P. Huber (2011), 1106.0687.
[6] G. Mention, M. Fechner, T. Lasserre, T. Mueller, D. Lhuillier, et al. (2011), 1101.2755.
[7] G. Karagiorgi, Z. Djurcic, J. Conrad, M. Shaevitz, and M. Sorel, Phys.Rev. **D80**, 073001 (2009), 0906.1997.
[8] J. Kopp, M. Maltoni, and T. Schwetz (2011), 1103.4570.
[9] C. Giunti and M. Laveder (2011), 1107.1452.
[10] C. Giunti and M. Laveder (2011), 1109.4033.
[11] G. Karagiorgi (2011), 1110.3735.
[12] L. M. Krauss, C. Lunardini, and C. Smith (2010), 1009.4666.
[13] E. Giusarma, M. Corsi, M. Archidiacono, R. de Putter, A. Melchiorri, et al., Phys.Rev. **D83**, 115023 (2011), 1102.4774.
[14] J. Hamann, S. Hannestad, G. G. Raffelt, and Y. Y. Wong, JCAP **1109**, 034 (2011), 1108.4136.
[15] N. Arkani-Hamed, D. P. Finkbeiner, T. R. Slatyer, and N. Weiner, Phys.Rev. **D79**, 015014 (2009), 0810.0713.
[16] P. Meade, M. Papucci, and T. Volansky (2009), 0901.2925.
[17] P. J. Fox and E. Poppitz (2008), 0811.0399.
[18] C. Cheung, J. T. Ruderman, L.-T. Wang, and I. Yavin (2009), 0902.3246.
[19] A. Katz and R. Sundrum, JHEP **0906**, 003 (2009), 0902.3271.
[20] A. E. Nelson and J. Walsh, Phys.Rev. **D77**, 033001 (2008), arXiv:0711.1363.
[21] N. Engelhardt, A. E. Nelson, and J. R. Walsh, Phys.Rev. **D81**, 113001 (2010), arXiv:1002.4452.
[22] G. Karagiorgi, M. Shaevitz, and J. Conrad (2012), 1202.1024.
[23] M. Pospelov (2011), 1103.3261.
[24] C. E. Aalseth et al. (CoGeNT) (2010), 1002.4703.

[25] C. Aalseth, P. Barbeau, J. Colaresi, J. Collar, J. Leon, et al. (2011), 1106.0650.
[26] G. Angloher, M. Bauer, I. Bavykina, A. Bento, C. Bucci, et al. (2011), 1109.0702.
[27] R. Bernabei, P. Belli, F. Cappella, R. Cerulli, C. Dai, et al., Eur.Phys.J. **C67**, 39 (2010), arXiv:1002.1028.
[28] N. Arkani-Hamed, S. Dimopoulos, and G. Dvali, Phys.Lett. **B429**, 263 (1998), hep-ph/9803315.
[29] T. G. Rizzo, Phys.Lett. **B665**, 361 (2008), 0805.0281.
[30] M. Drees, M. Hanussek, and J. S. Kim (2012), 1201.5714.
[31] A. Friedland, M. L. Graesser, I. M. Shoemaker, and L. Vecchi (2011), 1111.5331.
[32] Z. Ahmed et al. (CDMS-II Collaboration), Phys.Rev.Lett. (2010), 1011.2482.
[33] P. J. Fox, D. E. Kaplan, E. Katz, E. Poppitz, V. Sanz, et al. (2005), hep-th/0503249.
[34] T. B. Collaboration (2011), 1104.1816.
[35] B. Aharmim et al. (SNO), Phys. Rev. **C72**, 055502 (2005), nucl-ex/0502021.
[36] B. Aharmim et al. (SNO Collaboration), Phys.Rev. **C81**, 055504 (2010), 0910.2984.
[37] J. Engel, Phys.Lett. **B264**, 114 (1991).
[38] J. Kopp, V. Niro, T. Schwetz, and J. Zupan, Phys. Rev. **D80**, 083502 (2009), 0907.3159.
[39] E. Aprile, K. Arisaka, F. Arneodo, A. Askin, L. Baudis, et al. (2011), 1101.3866.
[40] R. Bernabei et al. (DAMA), Eur. Phys. J. **C56**, 333 (2008), 0804.2741.
[41] P. F. Sorensen, Ph.D. thesis, Brown University (2008).
[42] A. Beda, E. Demidova, A. Starostin, V. Brudanin, V. Egorov, et al., Phys.Part.Nucl.Lett. **7**, 406 (2010), 0906.1926.
[43] J. N. Bahcall, A. M. Serenelli, and S. Basu, Astrophys.J. **621**, L85 (2005), Solar model data available from http://www.sns.ias.edu/∼jnb/, astro-ph/0412440.
[44] C. Arpesella et al. (Borexino Collaboration), Phys.Lett. **B658**, 101 (2008), arXiv:0708.2251.
[45] C. Arpesella et al. (The Borexino Collaboration), Phys.Rev.Lett. **101**, 091302 (2008), arXiv:0805.3843.
[46] W. Marciano and A. Sanda, Phys.Lett. **B67**, 303 (1977).
[47] C. Giunti and A. Studenikin, Phys.Atom.Nucl. **72**, 2089 (2009), 0812.3646.
[48] J. E. Kim, Phys.Rev. **D14**, 3000 (1976).
[49] M. Beg, W. Marciano, and M. Ruderman, Phys.Rev. **D17**, 1395 (1978).
[50] H. Georgi and L. Randall, Phys.Lett. **B244**, 196 (1990).
[51] M. Czakon, J. Gluza, and M. Zralek, Phys.Rev. **D59**, 013010 (1999).
[52] R. Mohapatra, S.-P. Ng, and H.-b. Yu, Phys.Rev. **D70**, 057301 (2004), hep-ph/0404274.
[53] K. Nakamura et al. (Particle Data Group), J. Phys. **G37**, 075021 (2010).
[54] J. F. Beacom and P. Vogel, Phys.Rev.Lett. **83**, 5222 (1999), hep-ph/9907383.
[55] A. S. Joshipura and S. Mohanty, Phys.Rev. **D66**, 012003 (2002), hep-ph/0204305.
[56] W. Grimus, M. Maltoni, T. Schwetz, M. Tortola, and J. Valle, Nucl.Phys. **B648**, 376 (2003), hep-ph/0208132.
[57] G. Raffelt, Phys.Rept. **320**, 319 (1999).
[58] A. Kuznetsov, N. Mikheev, and A. Okrugin, Int.J.Mod.Phys. **A24**, 5977 (2009), 0907.2905.
[59] P. Vogel and J. Engel, Phys.Rev. **D39**, 3378 (1989).
[60] M. Bordag, U. Mohideen, and V. Mostepanenko, Phys.Rept. **353**, 1 (2001), quant-ph/0106045.
[61] M. Bordag, G. Klimchitskaya, and U. Mohideen, *Advances in the Casimir effect*, International series of monographs on physics (Oxford University Press, 2009), ISBN 9780199238743, URL `http://books.google.ch/books?id=QQlKT41qWo8C`.
[62] E. Adelberger, B. R. Heckel, S. A. Hoedl, C. Hoyle, D. Kapner, et al., Phys.Rev.Lett. **98**, 131104 (2007), hep-ph/0611223.
[63] E. Adelberger, J. Gundlach, B. Heckel, S. Hoedl, and S. Schlamminger, Prog.Part.Nucl.Phys. **62**, 102 (2009).
[64] J. Redondo, JCAP **0807**, 008 (2008), 0801.1527.
[65] J. Jaeckel and A. Ringwald (2010), 1002.0329.
[66] J. B. Dent, F. Ferrer, and L. M. Krauss (2012), 1201.2683.
[67] B. Feldman and A. E. Nelson, JHEP **0608**, 002 (2006), hep-ph/0603057.
[68] A. D. Dolgov and G. G. Raffelt, Phys.Rev. **D52**, 2581 (1995), hep-ph/9503438.
[69] B. Aharmim, S. Ahmed, J. Amsbaugh, J. Anaya, A. Anthony, et al. (2011), 1107.2901.
[70] M. Ahlers, J. Jaeckel, J. Redondo, and A. Ringwald, Phys.Rev. **D78**, 075005 (2008), 0807.4143.
[71] B. Holdom, Phys.Lett. **B166**, 196 (1986).

[72] S. Davidson, S. Hannestad, and G. Raffelt, JHEP **0005**, 003 (2000), erratum added online, Oct/17/2000, hep-ph/0001179.
[73] A. Y. Smirnov and R. Zukanovich Funchal, Phys.Rev. **D74**, 013001 (2006), hep-ph/0603009.
[74] A. Kusenko, Phys.Rept. **481**, 1 (2009), 0906.2968.
[75] G. Gelmini, S. Palomares-Ruiz, and S. Pascoli, Phys.Rev.Lett. **93**, 081302 (2004), astro-ph/0403323.
[76] A. Nelson and J. Walsh, Phys.Rev. **D77**, 095006 (2008), arXiv:0802.0762.
[77] S. P. Mikheyev and A. Y. Smirnov, Nuovo Cim. **C9**, 17 (1986).
[78] L. Wolfenstein, Phys. Rev. **D17**, 2369 (1978).
[79] J. Collar (2011), talk at TAUP 2011, "12th International Conference on Topics in Astroparticle and Underground Physics", URL `http://taup2011.mpp.mpg.de/`.
[80] D. Tucker-Smith and N. Weiner, Phys. Rev. **D64**, 043502 (2001), hep-ph/0101138.
[81] S. Chang, R. F. Lang, and N. Weiner, Phys.Rev.Lett. **106**, 011301 (2011), 1007.2688.
[82] R. Bernabei et al., Phys. Lett. **B389**, 757 (1996).
[83] E. Aprile et al. (XENON100 Collaboration), Phys.Rev.Lett. (2011), 1104.2549.
[84] V. A. Kudryavtsev, M. Robinson, and N. J. C. Spooner (2009), 0912.2983.
[85] J. P. Ralston (2010), 1006.5255.
[86] D. Nygren (2011), 1102.0815.
[87] K. Blum (2011), 1110.0857.
[88] R. Bernabei, P. Belli, F. Cappella, V. Caracciolo, R. Cerulli, et al. (2012), 1202.4179.
[89] M. T. Frandsen, F. Kahlhoefer, J. March-Russell, C. McCabe, M. McCullough, et al. (2011), 1105.3734.
[90] T. Schwetz and J. Zupan (2011), 1106.6241.
[91] M. Farina, D. Pappadopulo, A. Strumia, and T. Volansky (2011), 1107.0715.
[92] P. J. Fox, J. Kopp, M. Lisanti, and N. Weiner (2011), 1107.0717.
[93] D. Hooper and C. Kelso (2011), 1106.1066.
[94] P. Belli, R. Bernabei, A. Bottino, F. Cappella, R. Cerulli, et al. (2011), 1106.4667.
[95] R. Bernabei, P. Belli, R. Cerulli, F. Montecchia, M. Amato, et al., Nuovo Cim. **A112**, 1541 (1999).
[96] S. Ahlen, N. Afshordi, J. Battat, J. Billard, N. Bozorgnia, et al., Int.J.Mod.Phys. **A25**, 1 (2010), 0911.0323.
[97] K. Freese, J. A. Frieman, and A. Gould, Phys.Rev. **D37**, 3388 (1988), see in particular figure 8 of that paper.
[98] J. Bahcall, *Neutrino astrophysics* (Cambridge University Press, 1989), ISBN 9780521351133, URL `http://books.google.com/books?id=gA5hQgAACAAJ`.
[99] E. K. Akhmedov, M. Tortola, and J. Valle, JHEP **0405**, 057 (2004), hep-ph/0404083.
[100] E. K. Akhmedov (1999), hep-ph/0001264.
[101] P. J. Fox, J. Liu, D. Tucker-Smith, and N. Weiner (2011), 1104.4127.
[102] NASA and J. A. Program, *Aster global digital elevation map, version 1* (2009), aSTER GDEM is a product of METI and NASA, URL `http://asterweb.jpl.nasa.gov/gdem.asp`.
[103] R. Bellotti et al. (MACRO Collaboration, EASTOP Collaboration), Phys.Rev. **D42**, 1396 (1990).
[104] N. Bozorgnia, G. B. Gelmini, and P. Gondolo (2010), 1006.3110.
[105] N. Bozorgnia, G. B. Gelmini, and P. Gondolo (2010), 1008.3676.
[106] N. Bozorgnia, G. B. Gelmini, and P. Gondolo (2010), 1009.3325.
[107] N. Bozorgnia, G. B. Gelmini, and P. Gondolo (2010), 1011.6006.
[108] N. Bozorgnia, G. B. Gelmini, and P. Gondolo (2011), 1101.2876.
[109] N. Bozorgnia (2011), 1109.0735.
[110] M. Pospelov, Phys. Rev. **D80**, 095002 (2009), 0811.1030.
[111] G. Bennett et al. (Muon G-2 Collaboration), Phys.Rev. **D73**, 072003 (2006), summary of E821 Collaboration measurements of the muon anomalous magnetic moment, each reported earlier in Letters or Brief Reports., hep-ex/0602035.
[112] J. D. Bjorken, R. Essig, P. Schuster, and N. Toro, Phys. Rev. **D80**, 075018 (2009), 0906.0580.
[113] B. Batell, M. Pospelov, and A. Ritz, Phys.Rev. **D80**, 095024 (2009), 0906.5614.
[114] R. Essig, R. Harnik, J. Kaplan, and N. Toro, Phys.Rev. **D82**, 113008 (2010), 1008.0636.
[115] S. Abrahamyan et al. (APEX Collaboration), Phys.Rev.Lett. **107**, 191804 (2011), 1108.2750.
[116] R. Essig, P. Schuster, and N. Toro, Phys.Rev. **D80**, 015003 (2009), 0903.3941.
[117] C. D. Carone and H. Murayama, Phys.Rev.Lett. **74**, 3122 (1995), hep-ph/9411256.
[118] M. L. Graesser, I. M. Shoemaker, and L. Vecchi (2011), 1107.2666.

[119] D. Bartlett and S. Loegl, Phys.Rev.Lett. **61**, 2285 (1988).
[120] G. G. Raffelt and G. D. Starkman, Phys.Rev. **D40**, 942 (1989).
[121] E. Arik et al. (CAST Collaboration), JCAP **0902**, 008 (2009), 0810.4482.
[122] M. Ahlers, H. Gies, J. Jaeckel, J. Redondo, and A. Ringwald, Phys.Rev. **D77**, 095001 (2008), 0711.4991.
[123] A. Mirizzi, J. Redondo, and G. Sigl, JCAP **0903**, 026 (2009), 0901.0014.
[124] D. Fixsen, E. Cheng, J. Gales, J. C. Mather, R. Shafer, et al., Astrophys.J. **473**, 576 (1996), astro-ph/9605054.
[125] A. Beda, V. Brudanin, V. Egorov, D. Medvedev, V. Pogosov, et al. (2010), 1005.2736.
[126] H. T. Wong, H.-B. Li, and S.-T. Lin, Phys.Rev.Lett. **105**, 061801 (2010), 1001.2074v1.
[127] M. Voloshin, Phys.Rev.Lett. **105**, 201801 (2010), 1008.2171.
[128] H. T. Wong, H.-B. Li, and S.-T. Lin, Phys.Rev.Lett. **105**, 061801 (2010), 1001.2074v3.
[129] J. Redondo and M. Postma, JCAP **0902**, 005 (2009), 0811.0326.
[130] M. Pospelov and J. Pradler (2012), 30 pages, 9 figures, 1203.0545.